Electrochemical Proton Storage: From Fundamental Understanding to Materials to Devices

Tiezhu Xu[1], Di Wang[1], Zhiwei Li[1], Ziyang Chen[1], Jinhui Zhang[1], Tingsong Hu[1], Xiaogang Zhang[1] ✉, Laifa Shen[1] ✉

HIGHLIGHTS

- Fundamental principles and advantages of electrochemical proton storage are briefly reviewed.

- Research progresses and strategies to promote the development of electrochemical proton storage based on various charge storage mechanisms, electrode materials, and devices are discussed and summarized.

- Challenges and perspectives of the next-generation electrochemical proton storage technology are discussed.

ABSTRACT Simultaneously improving the energy density and power density of electrochemical energy storage systems is the ultimate goal of electrochemical energy storage technology. An effective strategy to achieve this goal is to take advantage of the high capacity and rapid kinetics of electrochemical proton storage to break through the power limit of batteries and the energy limit of capacitors. This article aims to review the research progress on the physicochemical properties, electrochemical performance, and reaction mechanisms of electrode materials for electrochemical proton storage. According to the different charge storage mechanisms, the surface redox, intercalation, and conversion materials are classified and introduced in detail, where the influence of crystal water and other nanostructures on the migration kinetics of protons is clarified.

Several reported advanced full cell devices are summarized to promote the commercialization of electrochemical proton storage. Finally, this review provides a framework for research directions of charge storage mechanism, basic principles of material structure design, construction strategies of full cell device, and goals of practical application for electrochemical proton storage.

KEYWORDS Electrochemical proton storage; Rapid kinetics; Charge storage mechanism; Material design; Device construction
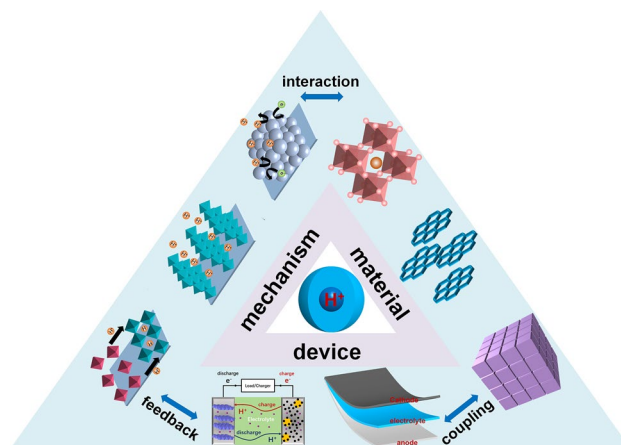
✉ Xiaogang Zhang, azhangxg@nuaa.edu.cn; Laifa Shen, lfshen@nuaa.edu.cn
[1] Jiangsu Key Laboratory of Electrochemical Energy Storage Technologies, College of Material Science and Technology, Nanjing University of Aeronautics and Astronautics, Nanjing 211106, People's Republic of China

1 Introduction

With the increase in demand for energy conversion and storage owing to the development of green energy technology, grid-scale energy storage is playing a more and more important role in the development of energy [1]. Electrochemical energy storage systems provide an effective strategy for improving the reliability and utilization of power grids [2]. Lithium-ion batteries (LIBs), as the best among them, have been widely studied all over the world. Recently, some promising metal batteries with lithium anodes have been the focus of research for higher energy density, such as Li–S batteries [3, 4], Li–O_2 batteries [5, 6], and Li–CO_2 batteries [7, 8]. However, the limitation of lithium resources and the strong demand for higher energy density and higher power density push the development of next-generation rechargeable batteries to replace current LIBs [9]. Therefore, a series of other metal ion charge carrier batteries have been developed, such as sodium-ion batteries (SIBs) [10], potassium-ion batteries (PIBs) [11], zinc-ion batteries (ZIBs) [12], magnesium-ion batteries (MIBs) [13], and aluminum-ion batteries (AIBs) [14]. Despite most of them deliver a high energy density, the power density of metal ion charge carrier batteries is very low due to the slow solid-state diffusion process during the electrochemical reaction. Furthermore, safety is also a common problem in metal ion charge carrier batteries, which limits their further development in some key areas. In order to meet the diverse demand for energy, various aqueous non-metal carrier batteries and supercapacitors with excellent electrochemical performance have become a hot topic in energy research [15–19].

Proton, the ion with the smallest molar mass, is an ideal charge carrier. Such a small ion mass will effectively decrease the mass burden of the electrode material, thereby leading to a higher capacity of the electrode [20]. For example, for a one-electron reaction in MoO_3, a hypothetical $HMoO_3$ electrode delivers a theoretical specific capacity of 185 mAh g^{-1}, which is higher than the theoretical specific capacity of $LiMoO_3$ (177 mAh g^{-1}) and $NaMoO_3$ (160 mAh g^{-1}). In addition, proton also has the smallest ionic radius ($\sim 10^{-15}$ m) and smaller hydrated ionic size (2.82 Å for H_3O^+), which contributes to the rapid migration of protons in electrolytes and electrodes. Typically, H_2SO_4 is one of the electrolytes with the highest ionic conductivity among all electrolytes. As early as 1802, Grotthuss proposed the Grotthuss conduction similar to Newton's cradle to explain the curious ion conductivity of acidic aqueous solutions [21]. Specifically, one water molecule combines with a proton and throws away another proton from the other end of the water molecule; then, the released proton is transferred to the next water molecule through a hydrogen-bonding chain, triggering a series of reorganizations of the hydrogen-bonding network and leading to the rapid transport of protons [22, 23]. Likewise, studies have shown that protons are transferred through hydrogen-bonding networks in hydrous oxides and MOFs following the Grotthuss mechanism [24, 25]. Different from obvious structural change in electrode material derived from intercalation of large-sized metal carriers during the charging and discharging process, the electrode structure distortion caused by protons with small ion radius can be ignored during the cycle. In summary, the superiority of proton carriers will endow electrochemical proton storage (EPS) with higher energy, fast chargeability, long cycle life, and other excellent electrochemical performance. In recent years, many proton batteries and pseudocapacitors with higher capacity, ultra-higher rate, and unparalleled cycle life have been reported [21, 26–30].

Unfortunately, although a lot of research has been done to develop EPS systems with excellent electrochemical performance in recent years, the huge gap between practical problems and ideal designs still restricts the practical application of EPS. At present, the development of electrode materials and the research of electrochemical reaction mechanisms for EPS are in their infancy, and it is still challenging to develop proton pseudocapacitors/batteries with fast charging capability and high stability. This article comprehensively reviews the development history of electrochemical proton storage materials and summarizes advanced electrochemical proton storage materials. These materials possess unique physicochemical properties compared with traditional electrode materials, which requires further understanding of the relationship between microstructure and electrochemical performance. This review also emphasizes the fundamental mechanism of electrochemical proton storage from atomic-scale electrochemistry, such as the law of charge transfer, the characteristic of proton transport, and the interaction mechanism between electrode materials and charge carriers. In order to develop high-performance devices, some advanced pseudocapacitors and batteries are discussed. From the perspective of experimental research and practical application,

the roadmaps for the mechanism research, the electrode design principles, and the commercialized application of the next-generation EPS are proposed.

2 Protons as Charge Carriers

2.1 Advantages of Electrochemical Proton Storage

To surpass the power limitations of metal ion charge carrier batteries and capacity limitations of electrical double-layer capacitors, more attention has been devoted to the research of non-metal ion charge carrier batteries. An electrochemical energy storage system that uses protons (H^+) as charge carriers is gradually appearing in people's vision, which is attributed to the following advantages: (i) excellent electrochemical performance, the proton has the smallest ionic radius and the smallest atomic mass, which can endow electrodes

with high energy density, fast kinetic reactions, and long cycle life when comparing with traditional charge carriers (Fig. 1a, c) [31]. (ii) Low cost, hydrogen is almost the most abundant element on earth (the percentage of hydrogen element is dozens of times higher than that of lithium element only in the Earth's crust), which directly reduces the cost (Fig. 1b). Moreover, the cost derived from the process of material preparation and equipment operation is greatly decreased, because proton batteries/pseudocapacitors mainly operate under a hydrous and oxygenic environment [32]. (iii) Environmental benignity, electrochemical proton storage systems frequently use acidic aqueous solutions as electrolytes to avoid the environmental pollution caused by the toxic organic electrolytes. (iv) Safety, active metals (such as Li, Na, and K) and flammable organic solvents are not used in EPS to reduce the occurrence of safety accidents such as spontaneous combustion. Specifically, proton batteries
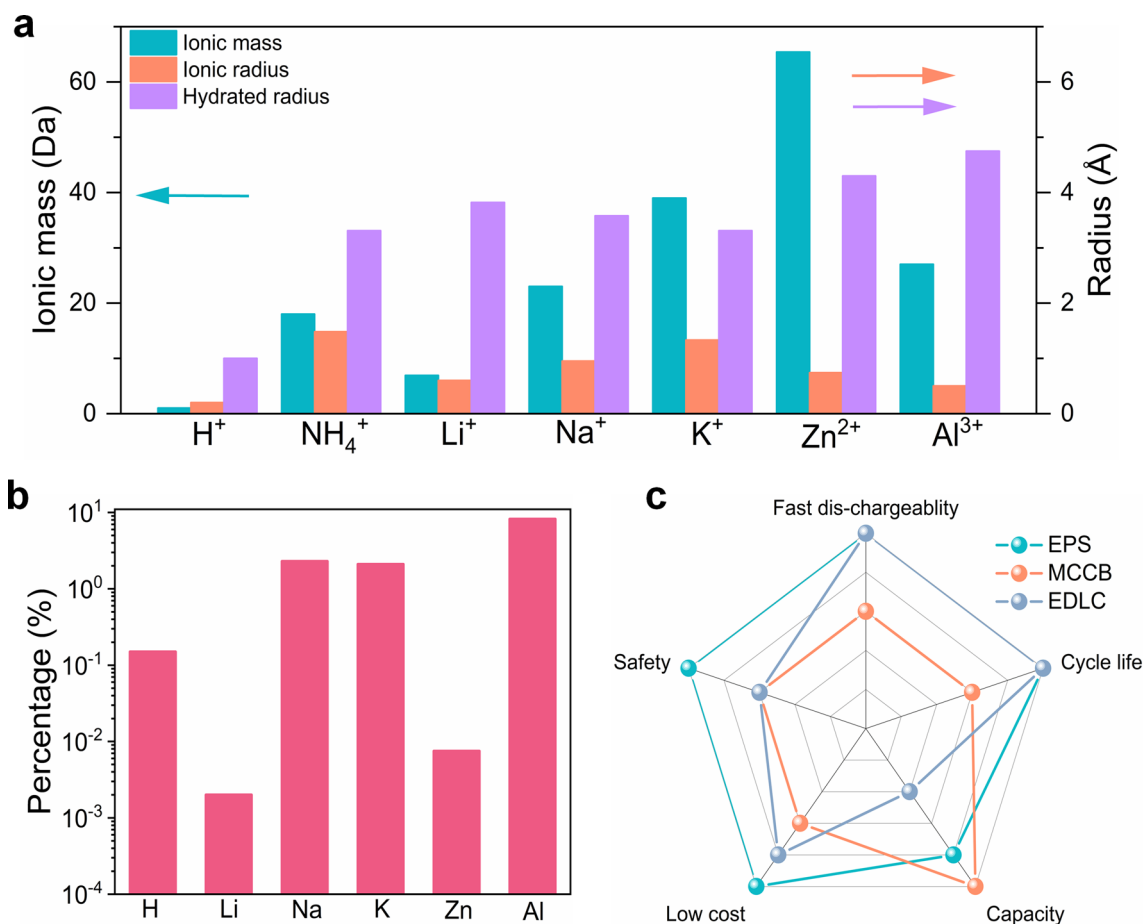
Fig. 1 **a** Ionic mass, ionic radius, and hydrated radius for typical cation charge carriers. **b** The abundance of various elements in the crust. **c** Radar plot comparing the property of different electrochemical energy storage systems, where EPS represents the electrochemical proton storage, MCCB represents metal ion charge carrier batteries, and EDLC represents electric double-layer capacitors

have been demonstrated to possess extremely outstanding electrochemical performance at especially low temperatures [33–40], which will be useful in military, polar, aerospace, and other fields.
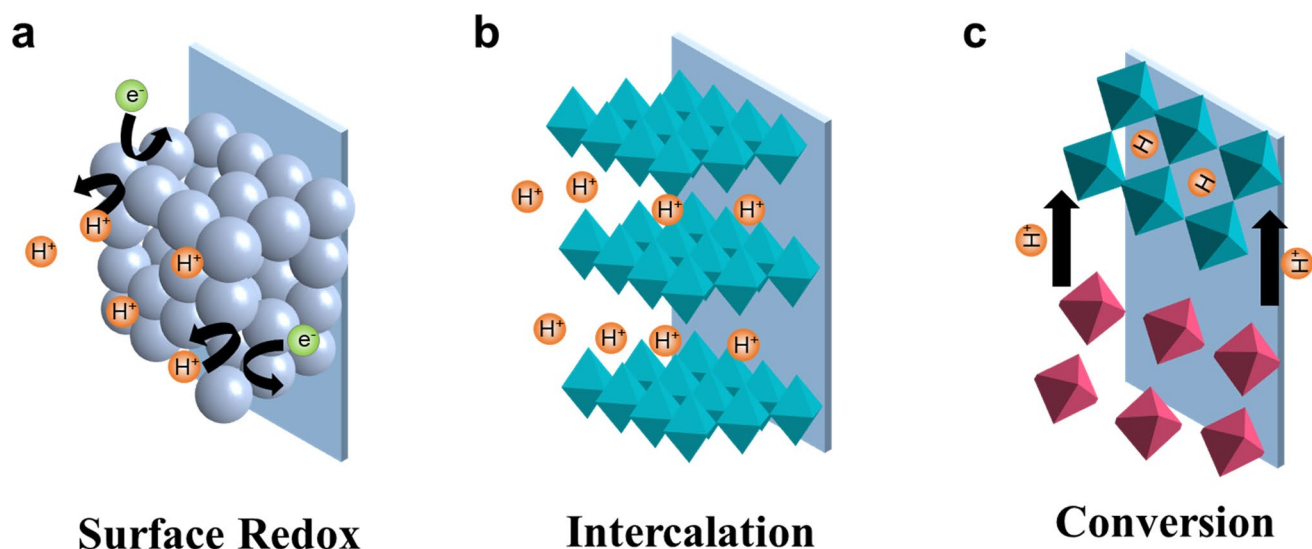
2.2 Electrochemical Proton Storage Mechanism

EPS is classified into three types based on their energy storage mechanisms: surface redox reaction mechanism, intercalation reaction mechanism, conversion reaction mechanism. (i) During the surface redox reaction, charge storage occurs on or near the electrode surface, leading to ideal capacitive behavior [41]. Protons will be electrochemically adsorbed, and a rapid kinetic reaction is completed in abrupt diffusion owing to the short diffusion distance (Fig. 2a). This surface redox reaction mechanism often occurs in RuO_2. (ii) For the intercalation reaction mechanism, protons are inserted into the electrode bulk phase and the electrode structure remains stable during the charging/discharging process, which ensures the electrode good cycle stability (Fig. 2b). In particular, intercalation reaction of metal ion charge carriers often progresses very slowly and is accompanied by a phase change (the main reason is that metal ions form ionic bonds with O or other anions in the electrode bulk phase). In contrast, the intercalation of protons is generally very rapid and undergoes a non-phase change (this is caused by the reason

that protons form covalent-ionic bonds with other atoms in the electrode bulk phase) [31]. According to the recent research, electrochemical proton storage materials based on intercalation reaction mechanisms are divided into the following categories: metal oxides (such as WO_3), two-dimensional transition metal carbides/nitrides (MXenes), and Prussian blue analogs (PBAs). (iii) Regarding the conversion reaction mechanism, the electrode materials will undergo structural conversion and chemical bond reorganization that is often accompanied by phase changes during the charging and discharging process, thereby releasing a huge capacity (Fig. 2c) [42]. Therefore, by breaking the limitation of the structure, the capacity of the conversion electrode material can be several times that of the intercalation-type material. Conversion electrode materials mainly include metal oxides (MoO_3) and organic materials (quinones, conductive polymers, covalent organic framework, etc.).

3 Electrochemical Proton Storage Materials and Mechanisms

Electrode materials are important compositions for electrochemical proton storage, ideal electrode materials should have the following characteristics: (i) large capacity and wide potential window, (ii) fast proton transport kinetics, (iii) long cycle life, (iv) low cost and pollution. Currently,

Fig. 2 Illustration of three types of charge storage mechanisms for electrochemical proton storage. **a** Surface redox reaction mechanism. **b** Intercalation reaction mechanism. **c** Conversion reaction mechanism

electrode materials for electrochemical proton storage have been initially developed, it is necessary to summarize and classify reported electrode materials to provide more valuable information for readers and researchers. Based on different charge storage mechanisms, electrode materials can be classified into surface redox reaction materials (RuO_2), intercalation reaction materials (WO_3, PBAs, and MXenes), and conversion reaction materials (MoO_3 and some organic materials) according to the recent research. In this section, the basic properties of electrode materials and the interaction mechanism between electrode materials and protons are mainly discussed.

3.1 Surface Redox Reaction Materials

RuO_2 is a classic material based on the surface redox reaction mechanism. In 1995, Zheng et al. reported for the first time that the electrochemical performance of RuO_2 depended on its crystal structure [43]. The amorphous phase-hydrated RuO_2 possessed a specific capacitance of 720 F g^{-1}, while the specific capacitance of highly crystalline $RuO_2 \cdot nH_2O$ was only about one-tenth of the former. Additionally, they also found that protons intercalated into the bulk of hydrous RuO_2 more easily than RuO_2 with the

crystalline phase due to the presence of water molecules in hydrous RuO_2. Dmowski et al. further revealed the influence of $RuO_2 \cdot nH_2O$ structure on physical and chemical properties by X-ray diffraction (XRD) and atomic pair density function (PDF) [44]. They found that the capacitance of $RuO_2 \cdot nH_2O$ was closely related to structural water content (when $n = 0.58$, $RuO_2 \cdot 0.58H_2O$ achieved a maximum capacitance of 850 F g^{-1}), and the changes of water content directly affected electronic and protonic penetration pathways. Furthermore, the PDF results indicated that the metallicity of hydrated RuO_2 came from the anhydrous rutile-like nanocrystals of RuO_2 and crystal water provided an efficient transport network for protons. Such nanostructure and crystal water endowed hydrated ruthenium oxide with not only high proton conductivity but also high electronic conductivity, pushing that $RuO_2 \cdot nH_2O$ was widely used in the energy storage and conversion field. More importantly, this also provided important ideas for the design of proton–electron mixed conductors and proton capacitive materials.

Yoshida et al. used small-angle X-ray diffraction (SAXA) to quantitatively study the relationship between RuO_2 sub-nanostructure and surface area and successfully revealed the origin of pseudocapacitance [45]. Specifically, the agglomeration state and specific surface area of
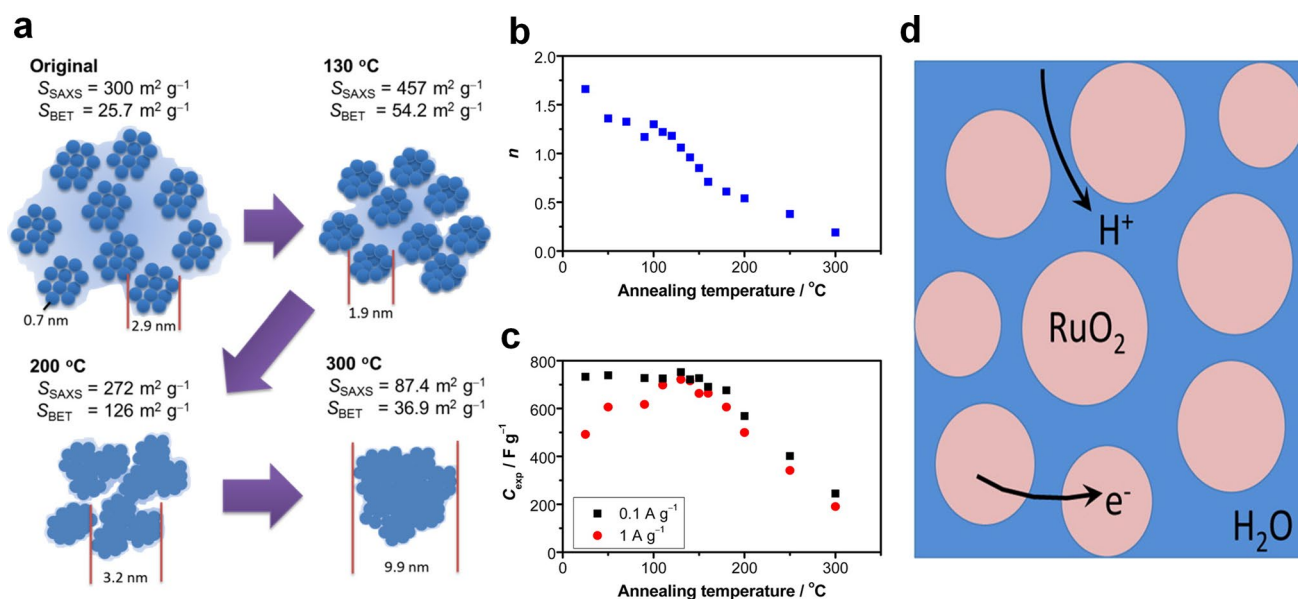
Fig. 3 **a** The relationship between specific surface area and particle size of $RuO_2 \cdot nH_2O$. **b** Water molecule content of $RuO_2 \cdot nH_2O$ at different annealing temperatures. **c** Specific capacitance of $RuO_2 \cdot nH_2O$ at different annealing temperatures [45]. Copyright 2013, American Chemical Society. **d** Schematic of proton charge transfer mechanism on RuO_2 surface. Ruthenium, oxygen, and hydrogen ions are shown as blue, red, and pink circles, respectively [46]. Copyright 2013, American Chemical Society

RuO_2 particles were different at different annealing temperatures (Fig. 3a), and the specific capacitance increased with the increase of the specific surface area of the material (the specific capacitance was 720 F g^{-1} at 457 m^2 g^{-1}, while the specific capacitance was less than 600 F g^{-1} at 272 m^2 g^{-1}) (Fig. 3b–c). The above results proved that the pseudocapacitance of RuO_2 came from the surface redox reaction, not the bulk reaction of RuO_2. In order to better understand the charge storage mechanism of RuO_2 in acidic media, more and more researchers have begun to use theoretical calculation methods to analyze the thermodynamic and kinetic behavior of RuO_2 on the atomic scale [46–49]. The results of first-principles density-functional theory (DFT) showed that the intercalation of protons would lead to the formation of O–H covalent bonds and the formation of an electronic delocalization state for only 0.3 electrons transferring to the Ru atom center. When the voltage was lower than 0.1 V, the energy barrier of proton

migration reached 1.8 eV, which demonstrated that the kinetics of protons were controlled by diffusion. When the voltage shifted to a higher voltage, additional protons tended to be adsorbed on the active sites of the RuO_2 surface to form functional groups such as hydroxyl groups (−OH). Overall, these conclusions support that unusual pseudocapacitance of RuO_2 comes from the charge transfer of protons on the grain boundary formed by water molecules and RuO_2 (Fig. 3d).

3.2 Intercalation Reaction Materials

3.2.1 WO₃

WO_3 is a typical oxide that crystallizes with the ReO_3-type structure (only ReO_3 and WO_3 in binary oxides) [50], which includes a WO_6 octahedral network with shared angles in three dimensions and a W–O–W bond angle of
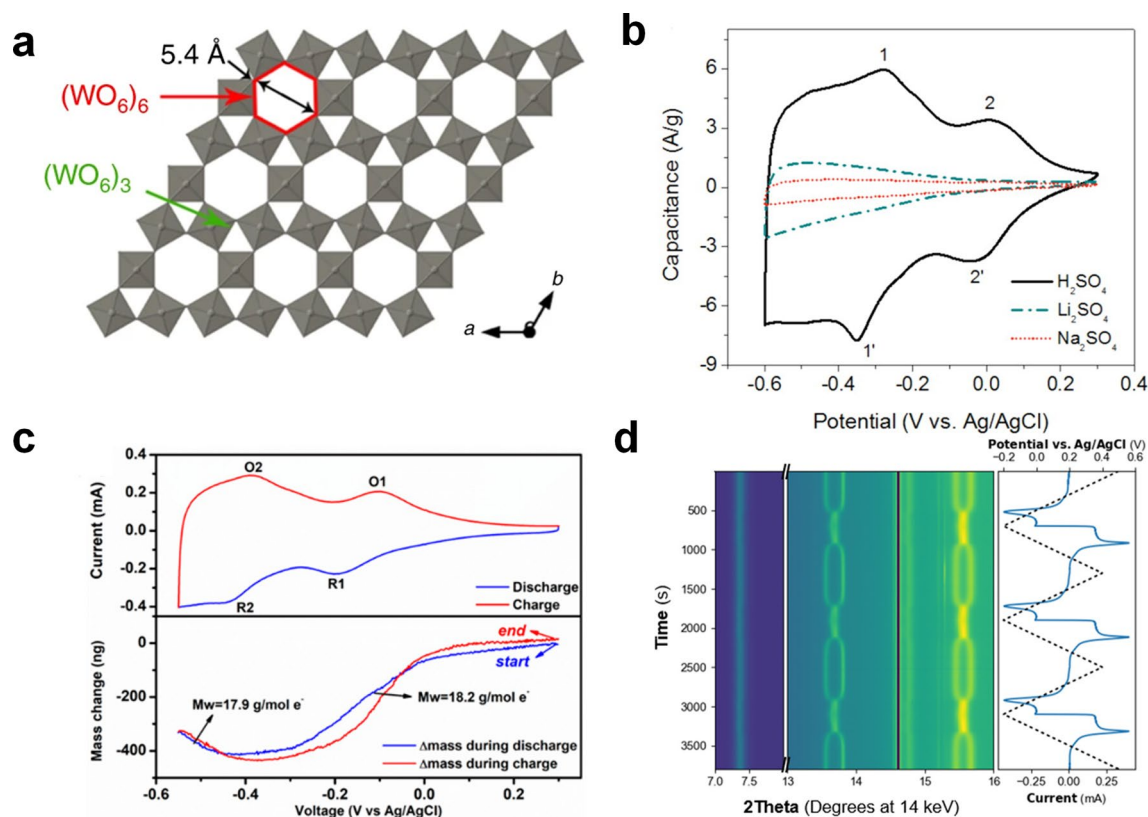
Fig. 4 a Schematic diagram of the electronic structure of h-WO_3 [59]. Copyright 2019, Springer Nature. b CV curves of h-WO_3·0.6H$_2$O in different electrolytes [26]. Copyright 2015, American Chemical Society. c The CV curves (top) and corresponding EQCM curves (bottom) of h-WO_3·0.6H$_2$O at 3 mV s^{-1} [63]. Copyright 2018, American Chemical Society. d In situ XRD study of electrochemical phase transition of WO_3·2H$_2$O at 1 mV s^{-1} [67]. Copyright 2019, American Chemical Society

between 165° and 179° [51]. Additionally, compared with other perovskite-type structures, the more open structure of ReO_3-type tungsten oxide is conducive to the intercalation and extraction of various charge carriers (Fig. 4a) [52]. WO_3 was initially used in the research of electrochromism where WO_3 film exhibited better color-changing ability, resulting from the co-intercalation of protons and electrons in H_2SO_4 solution [53–56], which made it possible for WO_3 to be used in electrochemical proton storage. Similar to $RuO_2 \cdot nH_2O$, crystal waters play an important role in the superfast transport of protons and the increase of specific capacity [57]. Mitchell et al. found that the presence of crystal water seriously affected the electrode reaction kinetics, and the electrochemistry reaction changed from battery to pseudocapacitive behavior with the change of crystal water content [58]. Particularly, $WO_3 \cdot 2H_2O$ electrode delivered a specific areal capacitance of 0.25 F cm^{-2} at a high loading mass of 4.57 mg cm^{-2} (charging or discharging only took 5 s). Chen et al. reported a hydrated h-WO_3 with high proton conductivity ($\sigma_H \sim 1$ mS cm^{-1}) and electronic conductivity ($\sigma_e \sim 0.6$ S cm^{-1}), possessing excellent electrochemical performance [26]. On the one hand, high specific capacitance (498 F g^{-1}) of h-WO_3 was derived from high specific surface area and open channels [59, 60]. On the other hand, the rapid migration of protons and electrons led to ultrahigh rate performance (over 80% capacitance retention at 100 mV s^{-1}). Additionally, the capacitance was almost not attenuated after 50,000 cycles because of the negligible strain caused by protons with small volumes in the electrode. Due to the excellent physical and chemical properties of WO_3 materials, the application of WO_3-based EPS in photoelectric integration and thermoelectric integration will be the direction of vigorous development in the future [61, 62].

However, the charge storage mechanism of tungsten oxide in acidic media is still controversial [59, 63–66]. The first crucial question is whether ions inserted into the electrode material are only protons (maybe H_3O^+ or even water molecules). Jiang et al. used a quartz crystal microbalance (QCM) to probe the relationship between mass changes and charge changes during the charge and discharge of h-$WO_3 \cdot 0.6H_2O$ [63]. They found that the reaction process was not a simply proton intercalation process, but involved multi-step reactions and the intercalation of a variety of ions (Fig. 4c). For a protonation process: first, $WO_3 \cdot 0.6H_2O$ absorbed ~0.29 H_2O when it came into contact with the electrolyte; secondly, the electrode excluded ~0.25 H_2O and acquired ~0.25 H^+;

then, ~0.3 H^+ was inserted into the electrode; finally, an intercalation process of ~0.17 H_3O^+ was found. Besides, another important question is what kind of role lattice water plays in the electrochemical reaction process. Many studies assumed that protons could be transported through the Grotthuss mechanism in materials with structural water, indicating that protons can jump very quickly on the hydrogen bond network. Wang et al. used operando atomic force microscopy dilatometry to detect the degree of deformation of WO_3 and $WO_3 \cdot 2H_2O$ during the redox process [66]. They found that the deformation of $WO_3 \cdot 2H_2O$ was lower than anhydrous WO_3 at a scan rate of 20 or 200 mV s^{-1}. (This corresponded to the better kinetics behavior of $WO_3 \cdot 2H_2O$.) Furthermore, by analyzing the local structural deformation rate combined with ex situ XRD, they revealed that the distortion of WO_3 was three-dimensional, while the distortion of $WO_3 \cdot 2H_2O$ was two-dimensional because of the presence of structural water. In order to understand the function of structural water in proton transport and faraday reaction, Mitchell et al. used operando XRD technology and solid-state nuclear magnetic resonance (SSNMR) to monitor the electrochemistry process of proton intercalation/de-intercalation in $WO_3 \cdot nH_2O$ and WO_3 [67]. The two pairs of (200)/(001) and (101)/(011) diffraction peaks of hydrated WO_3 were highly reversible during charging and discharging at a scan rate of 1 and 100 mV s^{-1}, demonstrating that $WO_3 \cdot 2H_2O$ had a reversible phase transition during the de/intercalation of protons (Fig. 4d). On the contrary, the structure of WO_3 could not respond quickly to electrochemical protons intercalation because there was no obvious structural transformation of WO_3 at 100 mV s^{-1}. Thus, the above conclusions not only proved that the structural water ensured the stability of electrode structure and accelerated the reaction kinetics of electrode, but also provided a novel strategy for the development of high-power energy storage devices via taking advantage of the flexibility of confined fluids.

3.2.2 Prussian Blue Analogues (PBAs)

Prussian blue analogues (PBAs) are a class of substances with a molecular formula $A_xM_1[M_2(CN)_6] \cdot_y \square_{1-y} \cdot zH_2O$, where A represents alkali metal element (such as K, Na, and Li), M is transition metal element (M_1 may be Fe, Mn, Zn, etc., while M_2 usually is Fe, Co or Mn), $\square$ represents vacancy, and water molecules are mainly divided into free
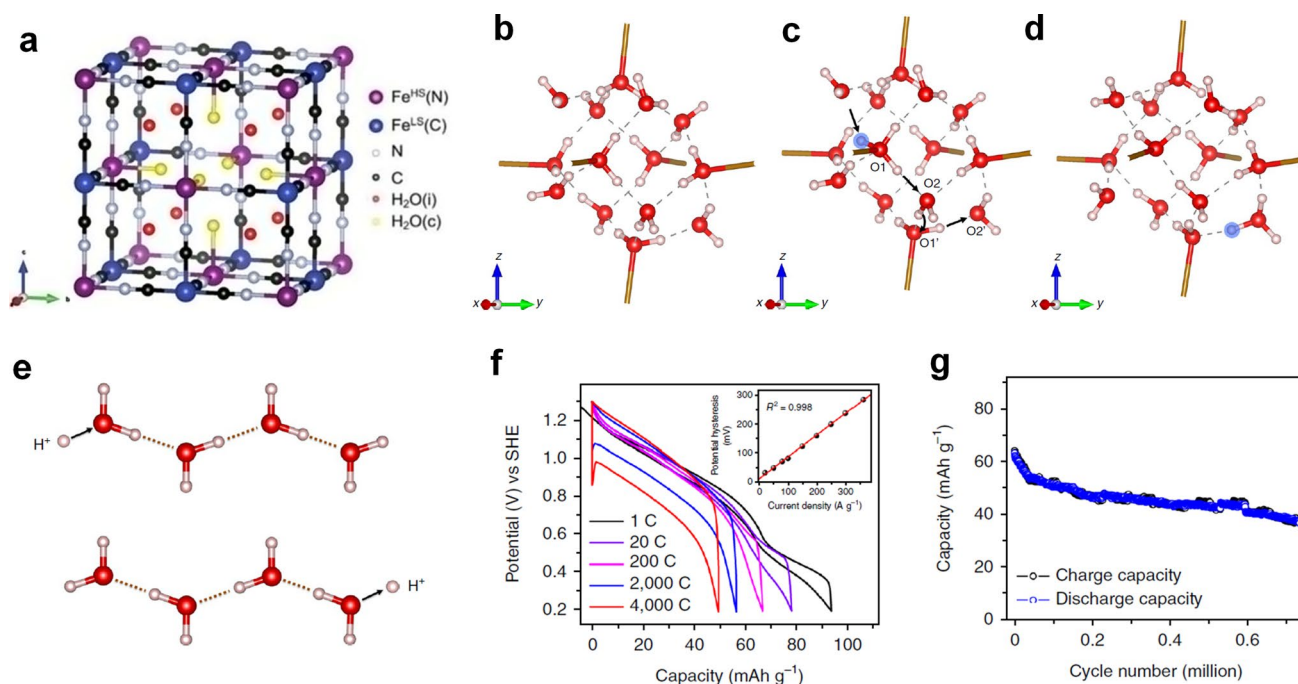
Fig. 5 **a** Schematic of crystal structure of $Fe_4[Fe(CN)_6]_3·14H_2O$ [68]. Copyright 2020, Wiley–VCH. **b–d** The transport path of protons in CuFe-TBA. **e** Schematic of Grotthuss mechanism. **f** GCD curves of CuFe-TBA at different current rates. **g** Cycle performance of CuFe-TBA at a current density of 500 C [21]. Copyright 2019, Springer Nature

water, coordination water, and zeolite water (Fig. 5a) [68, 69]. These ions and molecules are alternately connected to each other to form a cubic open frame. Additionally, rigid crystal lattices and open-dimensional tunnels facilitate charge carriers diffusion in PBAs, leading to widespread use of PBAs in the field of electrochemical energy storage [21, 38, 70–75]. However, PBAs prepared by the liquid deposition method suffer from poor crystallinity (the presence of defects and water molecules), resulting in that PBA-based metal ion charge carrier batteries often exhibit poor cycle life [70]. For most batteries, increasing crystallinity and reducing water content are the key strategy to improve the electrochemical performance of PBAs. It is thought-provoking that many previous studies have demonstrated that crystal water is of great significance to the transport of protons, so the structure design of electrodes for proton batteries should be quite different from conventional PBAs [76, 77]. Simultaneously, some studies have found that PBAs based on the Grotthuss mechanism had high proton conductivity due to the existence of a 3D hydrogen bond network formed between zeolite water [77, 78]. Wu et al. demonstrated that only CuFe-TBA with a continuous hydrogen bond network

was the best host for proton storage, of which zeolite water and ligand water formed hydrogen bonds and connected them together to build a penetration hydrogen bond network when there were vacancies in adjacent sites [21]. The DFT calculation was used to track the migration of protons in the intercalation process: they first modeled protons combined with ligand water after entering, and then protons appeared in the position of the zeolite water after relaxation, indicating that zeolite waters were the best binding sites for protons (Fig. 5b–d). Besides, protons were transported through cooperative cleavage and reconstruction of the covalent and hydrogen bond, resulting in 0.15 eV activation energy, which indicated that the Grotthuss mechanism played a key role in the transport and storage of protons in CuFe-TBA (Fig. 5e). Finally, the CuFe-TBA electrode achieved super rate performance (the electrode delivered a specific capacity of 49 mAh g^{-1} at 4000 C) and unprecedented cycle life (capacity retention was 60% after 0.73 million cycles at 500 C) (Fig. 5f–g). Taking advantage of Grotthuss topochemistry will facilitate the effective combination of batteries and capacitors and provide new ideas for the development of high-energy and high-power electrochemical energy storage devices.

In addition, another Turnbull blue analog (NiFe-TBA) had also been reported, the NiFe-TBA cathode achieved an ultrahigh rate performance at 6000 C (390 A g^{-1}) and a high capacity at -40 °C [38]. Moreover, they used operando synchrotron XRD to evolve the proton reaction process, during charge and discharge only a slight shift occurred at a diffraction angle (200) (corresponding to the mutual conversion between $[Fe^{II}(CN)_6]^{4-}$ and $[Fe^{III}(CN)_6]^{3-}$). In situ X-ray absorption near-edge spectra (XANES) revealed that the valence state of Fe had changed, but the valence state of Ni had not changed in the whole process, which identified that Fe was the active center of the electrochemical reaction. Although PBAs have outstanding advantages in proton battery applications, low capacity is still a problem to be solved. On the other hand, V-based PBAs may be used as electrode materials for high-capacity proton batteries owing to the high theoretical capacity of V-based compounds and the multi-electron reaction of V elements [72]. Peng et al. reported a vanadium hexacyanoferrate (VHCF) with a high capacity of 108 mAh g^{-1} that was currently the highest capacity reported for PBA-based cathode electrode

for proton batteries [75]. The high capacity of VHCF mainly came from two redox active centers of vanadium ($V^{III} \leftrightarrow V^{IV} \leftrightarrow V^{V}$) and iron ($Fe^{II} \leftrightarrow Fe^{III}$). Nevertheless, it was a pity that the VHCF did not display an outstanding rate and long cycle life compared with TBAs, the reason for which could be the lack of a continuous hydrogen bond network and the water solubility of vanadium-based PBAs. To summarize, there is still a lot of work to be done to increase the capacity of PBAs and reveal the transport and storage mechanism of protons.

### 3.2.3 Two-dimensional Transition Metal Carbides/Nitrides (MXenes)

In 2011, an unprecedented 2D material MXene was reported [79]. Notably, MXenes are synthesized by HF acid etching MAX phase ($M_{n+1}AX_n$, where $n = 1, 2, 3$, M is transition metal such as Ti and Mo, A is often group 13 or group 14 element, and X represents carbon or nitrogen) (Fig. 6a). Consequently, the unique structure of MXenes endows them with excellent electrochemical performance: On the one hand, the presence of internal metal carbides increases
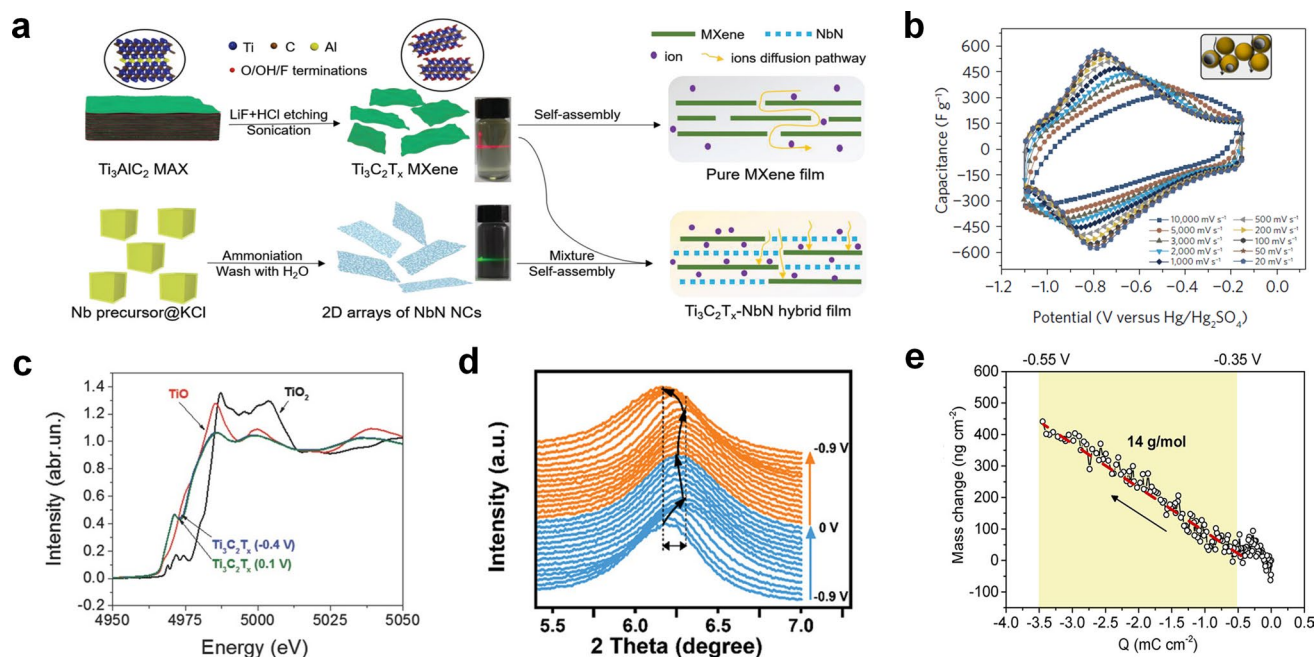
Fig. 6 **a** Diagram of structure and synthesis of MXene nanosheets [118]. Copyright 2020, Wiley–VCH. **b** Capacitance of macroporous Ti$_3$C$_2$T$_x$ electrode at various scan rates in 3 M H$_2$SO$_4$ [27]. Copyright 2017, Springer Nature. **c** Ti K-edge XANES spectra of Ti$_3$C$_2$T$_x$ at -0.4 and 0.1 V [83]. Copyright 2015, Wiley–VCH. **d** Electrochemical in situ X-ray diffraction study of Ti$_3$C$_2$T$_x$ in 1 M H$_2$SO$_4$ [85]. Copyright 2019, Wiley–VCH. **e** MXene electrode mass and response charge changes in 3 M H$_2$SO$_4$ [86]. Copyright 2020, American Chemical Society

electrochemically active sites to realize the rapid transfer of electrons; on the other hand, the two-dimensional nanostructure and structural waters existing between the layers can promote superfast transport of ions. Besides, abundant surface functional groups produced during the synthesis process provide a large number of redox active sites for protons. $Ti_3C_2T_x$, researched the most widespread among MXenes, has been comprehensively used in lithium-ion batteries [80], electric double-layer capacitors [81], pseudocapacitors [27], etc. In 2014, a method of preparing MXenes by etching MAX with a mixture of LiF and HF was reported by Ghidiu et al. (This reaction condition was milder than HF and beneficial to the decrease of nanosheet defects.) Additionally, a roller mill was used by them to mold a kind of high-conductivity 'clay' Ti_3C_2 film, which delivered high volumetric capacitance (900 F cm^{-3}), excellent cycle life, and rate performance in 1 M H_2SO_4. Aiming to overcome the limitation of rate and voltage for MXenes, Lukatskaya et al. prepared a macroporous MXene coated on a glassy carbon current collector [27]. The presence of glassy carbon effectively extended the electrochemical window to a breakthrough potential (-1.1 to -0.1 V versus Hg/Hg_2SO_4) in the acidic electrolyte, the reason for which could be that the higher overpotential of glassy carbon was beneficial to reducing hydrogen evolution reaction (HER). Simultaneously, the macroporous structure of the film provided a channel for the rapid transport of protons and enhanced the kinetics of the electrode (the electrode delivered a specific capacitance of 210 F g^{-1} at 10 V s^{-1}) (Fig. 6b). Furthermore, a 3 µm $Ti_3C_2T_x$ hydrogel electrode with a volumetric capacitance of 1500 F cm^{-3} that surpassed the volumetric capacity of all electrodes reported previously was found. In order to meet the actual demand for miniature devices and wearable electronic products, many MXene-based energy storage flexible devices have been developed. Unfortunately, inactive polymers (such as MMA) are often added into the electrode manufacturing process, resulting in a decrease in volumetric capacitance. Yu et al. took advantage of the excellent physical and chemical properties of antimonene (metal Sb nanosheets) to combine with MXene to form a uniform and dense high electroactive film, thereby improving the transport and storage of protons in MXene [82]. Finally, the specific capacity of the composite film had been greatly increased, and the volumetric capacitance value of 4255 F cm^{-3} was the largest value among the known MXene-based flexible electrodes.

Nevertheless, in sharp contrast to the vigorous development of MXene materials' structure design, there is still a lack of in-depth understanding of the excellent performance of MXene electrodes in acid electrolytes. MXene exhibits nearly rectangular cyclic voltammetry (CV) curves in a sulfuric acid electrolyte. (This is similar to the electrochemical behavior of RuO_2.) Lukatskaya et al. believed that such a high capacity was most likely to come from the intercalation pseudocapacitance rather than surface adsorption and desorption or surface redox [83]. To prove their hypothesis, they used X-ray absorption near edge structure spectroscopy (XANES) to detect the oxidation state changes of Ti elements at different potentials. The Ti edge shifted to lower energy as potential was negatively scanned from 0.275 to -0.35 V, and it would shift to higher energy when the potential was back to 0.35 V (Fig. 6c). Therefore, the electrochemical reaction can be assumed as:

$$Ti_3C_2O_x(OH)_yF_z + \delta H^+ + \delta e^- \leftrightarrow Ti_3C_2O_{x-\delta}(OH)_{y+\delta}F_z \quad (1)$$
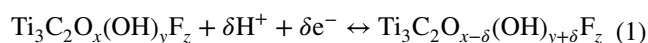
In the meantime, some studies had demonstrated that alkali metal cations in the electrolyte were inserted into $Ti_3C_2T_x$ layers and then bound to the ends of the functional groups on the surface of MXenes [84]. Generally, it was believed that the intercalation and extraction of protons will not cause major structural changes because of the minimum ion radius of protons. However, the charge storage of MXene in sulfuric acid was much more complicated when obvious lattice expansion/shrinkage was found by in situ XRD during charge and discharge [85]. The lattice parameter of the c-axis shrunk by 0.1 Å during discharging from 0 to -0.6 V and then expanded to 28.61 Å from 28.11 Å continued to discharge to -0.9 V (Fig. 6d). More importantly, DFT simulations showed that the interlayer spacing of $Ti_3C_2T_x$ with OH end groups expanded if proton inserted, while $Ti_3C_2T_x$ with O end groups shrunk after proton intercalation, these results were consistent with in situ XRD results. To understand the role of water molecules in charge storage of $Ti_3C_2T_x$, Shao et al. used a variety of in situ characterization techniques combined with molecular dynamics simulations to prove that hydronium ions instead of bare protons were inserted into electrodes during the electrochemical reaction (Fig. 6e) [86]. Besides, it was found that the presence of an appropriate amount of –OH would accelerate the reaction kinetics of $Ti_3C_2T_x$ electrodes. (Many –OH groups would destroy the structure of water molecules and slow down the transport

of ions, while few –OH groups would not be able to form a hydrogen bond network to trigger the Grotthuss mechanism.)

3.3 Conversion Reaction Materials

3.3.1 MoO₃

MoO_3 is a promising electrode material used in the battery field due to its extraordinary layered structure [87]. MoO_3 is most widely studied in the orthorhombic phase, monoclinic phase, and hexagonal phase, among which orthogonal MoO_3 (α-MoO_3) is most favored by researchers because of its unique physical and chemical properties [88]. In 2018, an α-MoO_3 electrode that delivered a discharge capacity of 152 mAh g^{-1} (5 C) in 1 M H_2SO_4 electrolyte was reported, and the capacity was 88 mAh g^{-1} at a rate of 100 C (Fig. 7a) [28]. Furthermore, the areal specific capacity reached 22.4 mAh cm^{-2} even under an ultra-high loading mass of 90 mg cm^{-2}, and such excellent areal specific capacity was never reported in other metal ion charge carrier batteries [89]. A free-standing $MoO_3/Ti_3C_2T_z$ composite film electrode also achieved high gravimetric/volumetric capacities of 837 and 1836 C cm^{-3} owing to MoO_3 nanobelts interconnected by MXene nanosheets [90]. However, it was puzzling that the redox peak in the CV curves was very sharp, unlike most electrochemical proton storage materials with a broad redox peak. Electrode kinetics studies showed that the kinetics of MoO_3 was limited by the diffusion of hydrogen ions ($b \approx 0.5$). Ex situ XRD was used to study the structural changes of the electrode during charging and discharging, a new phase $H_{0.84}MoO_3$ was generated with the emergence of some new peaks at 24.58°, 44.78°, and 48.28° from the initial potential to − 0.5 V (Fig. 7b). Then, new peaks appeared in pattern 3 and pattern 4 in the charging process, and the electrode returning to the initial potential was found to have a different structure from the initial structure (MoO_3), revealing that the first charge and discharge process was irreversible. The subsequent electrochemical reaction was highly reversible, which was why MoO_3 had a high-rate performance in acid electrolytes. The above reaction process was also confirmed by Yan et al. [40]. Nonetheless, although researchers
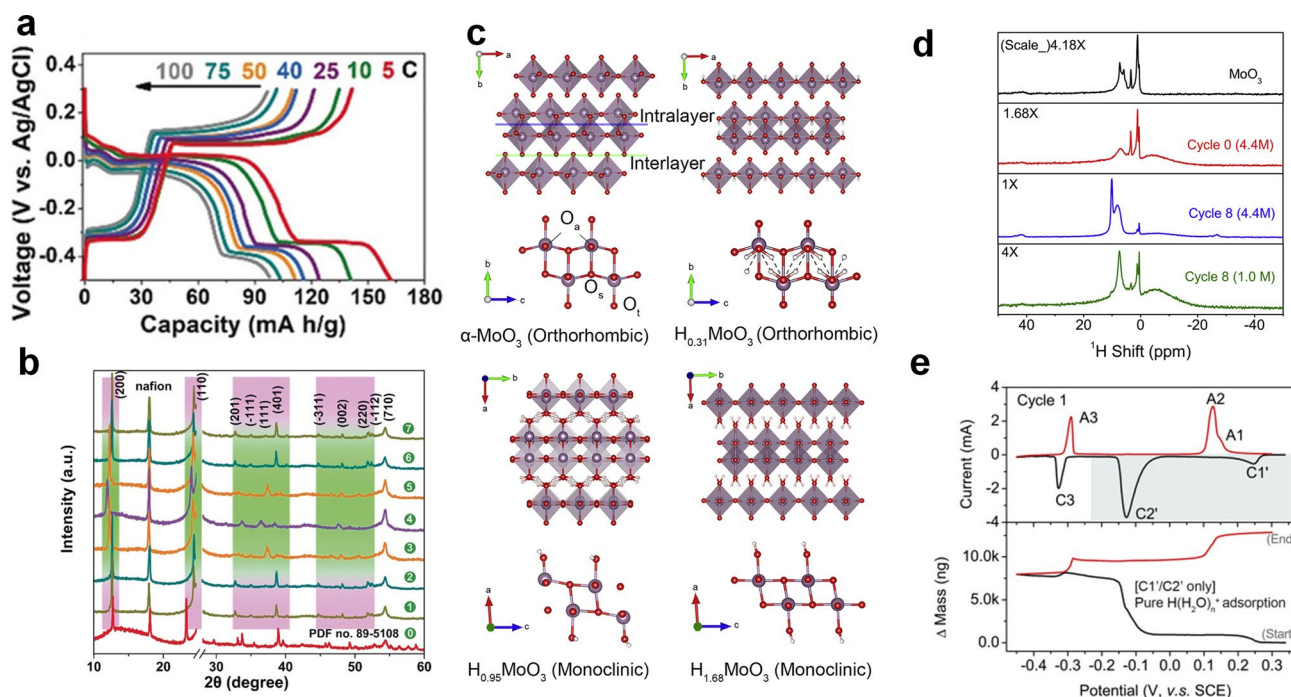

Fig. 7 a Rate performance of MoO₃ in 1 M H₂SO₄. **b** Ex situ XRD pattern of MoO₃ at different potentials [28]. Copyright 2018, Wiley–VCH. **c** Structural changes of α-MoO₃ during electrochemical reactions. **d** ¹H Solid-state NMR of original MoO₃ sample and cycled sample. **e** The CV and EQCM curves of MoO₃ electrode in the first cycle [91]. Copyright 2020, Elsevier

have already understood the structural changes of MoO_3 during charging and discharging, more subtle structural transformations require in situ characterization technique to identify. Guo et al. proved by in situ XRD that MoO_3 underwent many complex solid-solution reactions and two-phase reactions during charge and discharge (Fig. 7c) [91]. First, the following reactions occurred during the first discharge:

$$MoO_3 \rightarrow H_{0.31}MoO_3 \rightarrow H_{0.95}MoO_3 \rightarrow H_{1.68}MoO_3 \quad (2)$$
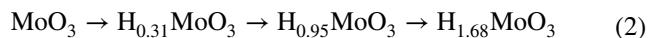
Then, the reaction process during the first charging process followed the following equation:

$$H_{1.68}MoO_3 \rightarrow H_{0.95}MoO_3 \rightarrow H_{0.5}MoO_3 \quad (3)$$
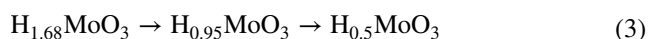
Finally, the following reversible electrochemical reaction occurred in the next cycles:

$$H_{0.5}MoO_3 \leftrightarrow H_{1.68}MoO_3 \leftrightarrow H_{0.95}MoO_3 \leftrightarrow H_{0.5}MoO_3 \quad (4)$$
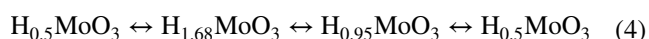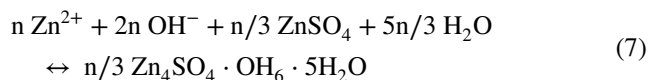
The above evidence also suggested that only intercalation/deintercalation of pure protons instead of water molecules or hydronium ions appeared in MoO_3 and hydrogen molybdenum bronzes (HMBs) during charging and discharging. What kind of role did water molecules play? Solid-state NMRs provided us with some information that hydronium ions only existed on the surface instead of the bulk lattice of the electrode (Fig. 7d). Simultaneously, the change of electrode mass that was detected by EQCM during the first two stages was caused by the adsorption of hydronium ions; then, water molecules stayed on the surface of the electrode and protons were inserted into the electrode material (Fig. 7e). During the charging process, protons were extracted from the bulk of the electrode with the opposite transport of water, causing a further increase in the mass of the electrode. As the content of absorbed and desorbed water molecules tended to be balanced, the charge transfer of the electrode was enhanced, and the electrode kinetics had been greatly improved by the synergistic effect of protons and water molecules.

3.3.2 Organic Materials

Organic materials, a type of conversion electrode materials, have been widely used in the field of energy storage for their low cost and diverse designability. Actually, the active sites of organic compounds can reversibly combine with protons in the electrolyte so that organic electrode materials can deliver higher specific capacity, but there are some problems such as poor conductivity and low stability [92]. A class of materials containing carbonyl functional groups (C=O) in organic compounds is used for electrochemical proton storage, such as benzoquinones and ketones [33, 93–95]. Two new redox-active bis- and terpolymers containing quinone-amine were synthesized by Navarro-Suarez et al., and the reaction between diamine and benzoquinone significantly enhanced the redox activity of polymers due to the generation of more active centers that were conducive to storaging more protons. Therefore, the poly(benzoquinone-co-hexamethyl-enediamine-co-PEO/PPO) electrode delivered a specific capacity of 230 mAh g^{-1} at a current density of 0.08 A g^{-1} (Fig. 8a) [94]. Moreover, it was revealed that the formation of intramolecular hydrogen bonds contributed to the transfer of protons and electrons via Fourier transform infrared spectroscopy (FTIR), facilitating the electrochemical reaction. Guo et al. also developed an organic pyrene-4,5,9,10-tetraone (PTO) that delivered a specific capacity of 208 mAh g^{-1} at 0.16 mA cm^{-2} as well as an outstanding rate performance of 85 mAh g^{-1} at 480 mA cm^{-2} [33]. Other organic electrode materials with C=N groups or N=N groups can also achieve reversible proton storage. A poly(2,9-dihydroquinoxalino[2,3-b] phenazine) (PO) organic material was synthesized to design an all-organic proton battery that delivered a specific capacity of 147 mAh g^{-1} with a long-term cycle life of over 500 cycles in mild electrolyte [96]. The chemical environments of adjacent C=N groups in PO molecules are different enough to result in a two-step redox reaction (Fig. 8b), PO molecules achieved reversible H^+ uptake/removal behavior in $ZnSO_4$ electrolyte:

$$2H_2O \leftrightarrow 2n\,H^+ + 2n\,OH^- \quad (5)$$

$$PO + 2n\,H^+ + 2n\,e^- \leftrightarrow P \quad (6)$$

$$n\,Zn^{2+} + 2n\,OH^- + n/3\,ZnSO_4 + 5n/3\,H_2O \\ \leftrightarrow n/3\,Zn_4SO_4 \cdot OH_6 \cdot 5H_2O \quad (7)$$

Besides, many conductive polymers (CPs) [97–99] and covalent organic frameworks (COFs) [100, 101] have been
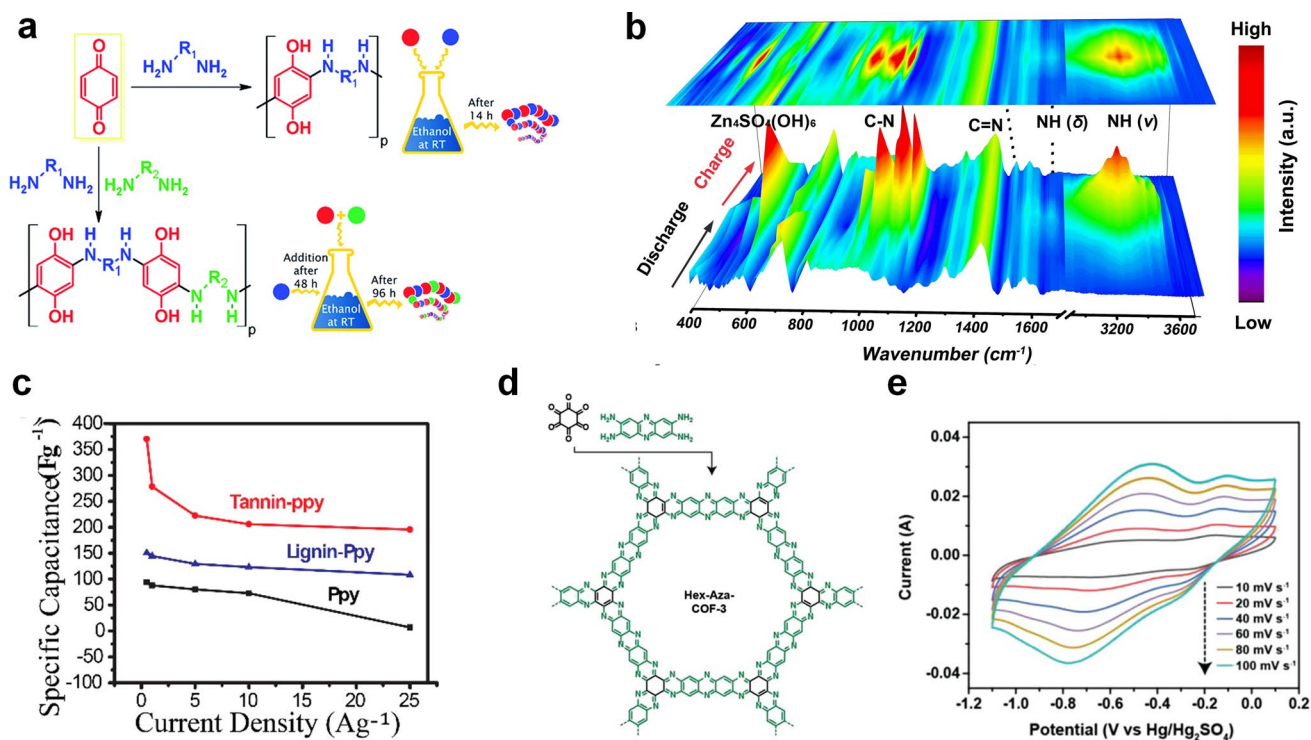
Fig. 8 **a** Schematic of preparation of bipolymer and terpolymer [94]. Copyright 2017, The Royal Society of Chemsitry. **b** Ex situ FTIR spectra of PO electrodes during charging and discharging process [96]. Copyright 2021, Wiley–VCH. **c** Specific capacitance of Tn/Ppy, Lig/Ppy, and Ppy at different current densities [97]. Copyright 2017, American Chemical Society. **d** The synthetic route of Hex-Aza-COF-3. **e** CV curves of Hex-Aza-COF-3 at various scan rates [100]. Copyright 2020, Wiley–VCH

developed as electrochemical proton storage materials. Conductive polymers with poor stability are often compounded with other substances to improve electrochemical performance. Mukhopadhyay et al. used environmentally friendly solvents to extract tannic acid with high phenol content (5.56 mol g^{-1}) from the bark [97]. The composite electrode of tannic acid and conductive polypyrrole (Ppy) achieved the highest specific capacitance of 370 F g^{-1} at a current density of 0.5 A g^{-1}, even the specific capacity remained 196 F g^{-1} at a high current density of 25 A g^{-1} (Fig. 8c). Likewise, a polypyrrole (PPy)/2D Cu-TCPP (TCPP = 5,10,15,20-tetrakis(4-carboxyphenyl)porphyrin) composite electrode with a compact composite network structure also achieved a specific capacitance of ~500 F g^{-1} in 0.5 M H$_2$SO$_4$ [98]. Covalent organic frameworks (COFs), a new type of crystalline organic porous materials, possess excellent structure, which endows them with great application potential in the fields of gas separation, photovoltaics, energy storage, catalysis, etc. [102]. Yang et al. designed two COFs with high crystallinity, stability, and porosity (NKCOF-2 and NKCOF-8), and the CNT/

NKCOF-2 composite electrode exhibited a specific capacity of 440 F g^{-1} at 0.5 A g^{-1}. FT-IR, PXRD, Raman spectroscopy, and EIS revealed that protons were transferred to active site (azo groups) via the Grotthuss conduction mechanism to achieve reversible conversion reactions (N=N + 2H$^+$ + 2e$^-$ ↔ H–N–N–H). Kandambeth et al. reported two kinds of COFs (Hex-Aza-COF-2 and Hex-Aza-COF-3), which were synthesized by cyclohexane-hexone and redox-functionalized aromatic tetramer with benzoquinone or phenazine in solvothermal condensation reaction (Fig. 8d) [100]. Unexpectedly, the electrochemical window of these two COFs electrodes in 1 M H$_2$SO$_4$ reached − 1 V (vs Hg/Hg$_2$SO$_4$), and the specific capacitance of Hex-Aza-COF-3 even achieved 663 F g^{-1}, which exceeded all reported COFs materials (Fig. 8e). The asymmetric device (RuO$_2$//Hex-Aza-COF-3) with a wide voltage of 1.7 V delivered an energy density of 23.3 Wh kg^{-1} at a power density of 661.2 W kg^{-1}. At present, the research on organic electrode materials for electrochemical proton storage is still in the preliminary stage, and further research on the synthesis, characterization,

Table 1 Summary of electrode materials for electrochemical proton storage

Material	Electrolyte	Potential (V)	Capacity (mAh g^{-1})	Rate (mAh g^{-1})	Cycle life (no. of cycles)	References
RuO$_2$·xH$_2$O	0.5 M H$_2$SO$_4$	0.2 to 1.2	417 (20 A g^{-1})	319 (150 A g^{-1})	–	[119]
RuO$_2$/Graphite	1 M H$_2$SO$_4$	0.2 to 1.2	173 (0.1 A g^{-1})	126 (20 A g^{-1})	5000 (80%)	[120]
WO$_3$·0.6H$_2$O	0.5 M H$_2$SO$_4$	−0.4 to 0.5	124 (5 mV s^{-1})	99 (100 mV s^{-1})	50,000 (100%)	[26]
H$_2$W$_2$O$_7$	3 M H$_2$SO$_4$	−0.2 to 0.8	70 (1 mV s^{-1})	56 (1 V s^{-1})	100,000 (89%)	[121]
CuFe-TBA	2 M H$_2$SO$_4$	0 to 1.3	95 (9.5 mA g^{-1})	49 (380 A g^{-1})	0.73 million (60%)	[21]
NiFe-TBA	1 M H$_2$SO$_4$	0 to 1.2	65 (0.1 A g^{-1})	39 (390 A g^{-1})	1000 (73%)	[38]
VHCF	6 M H$_2$SO$_4$	0.24 to 1.44	108 (0.1 A g^{-1})	65 (10 A g^{-1})	25,000 (92%)	[75]
Ti$_3$C$_2$T$_x$	3 M H$_2$SO$_4$	−0.45 to 0.55	125 (10 mV s^{-1})	58 (10 V s^{-1})	10,000 (90%)	[27]
n-F-Ti$_3$C$_2$T$_x$	3 M H$_2$SO$_4$	−0.2 to 0.4	87 (2 mV s^{-1})	–	10,000 (96%)	[122]
S-etched Ti$_3$C$_2$T$_x$	3 M H$_2$SO$_4$	−0.55 to 0.55	91 (5 mV s^{-1})	58 (10 V s^{-1})	10,000 (99%)	[123]
MoO$_3$	1 M H$_2$SO$_4$	−0.3 to 0.5	152 (0.2 A g^{-1})	88 (2 A g^{-1})	100 (67%)	[28]
MoO$_3$	6 M H$_2$SO$_4$	−0.26 to 0.54	235 (1 A g^{-1})	174 (40 A g^{-1})	5000 (87%)	[89]
Tn/Ppy	0.5 M H$_2$SO$_4$	0.3 to 0.9	62 (0.5 A g^{-1})	33 (25 A g^{-1})	~9000 (~100%)	[97]
PTO	2 M MnSO$_4$/H$_2$SO$_4$	0.2 to 0.9	208 (0.16 mA cm^{-2})	85 (400 mA cm^{-2})	1000 (67%)	[33]
Hex-Aza-COF-3	1 M H$_2$SO$_4$	−0.45 to 0.75	221 (1 A g^{-1})	–	–	[100]
CNT/NKCOF-2	2 M H$_2$SO$_4$	0 to 1.2	147 (0.5 A g^{-1})	72 (20 A g^{-1})	10,000 (91%)	[124]
NPenes	3 M HCl	0.2 to 1.2	395 (2 mV s^{-1})	–	–	[30]
2-GCE	2 M H$_3$PO$_4$	−0.5 to 0.65	284 (15 A g^{-1})	57 (15 A g^{-1})	–	[125]
W$_2$N	1 M H$_2$SO$_4$	−0.4 to 0.8	159 (2 mA cm^{-2})	99 (20 mA cm^{-2})	10,000 (92%)	[29]

All potentials are referenced to a standard hydrogen electrode (where Ag/AgCl vs. SHE = 0.2 V, Hg/Hg$_2$Cl$_2$ vs. SHE = 0.24 V, and Hg/Hg$_2$SO$_4$ vs. SHE = 0.65 V). Specific capacitance is converted to specific capacity by the following equation: $C = \frac{3.6Q}{V}$
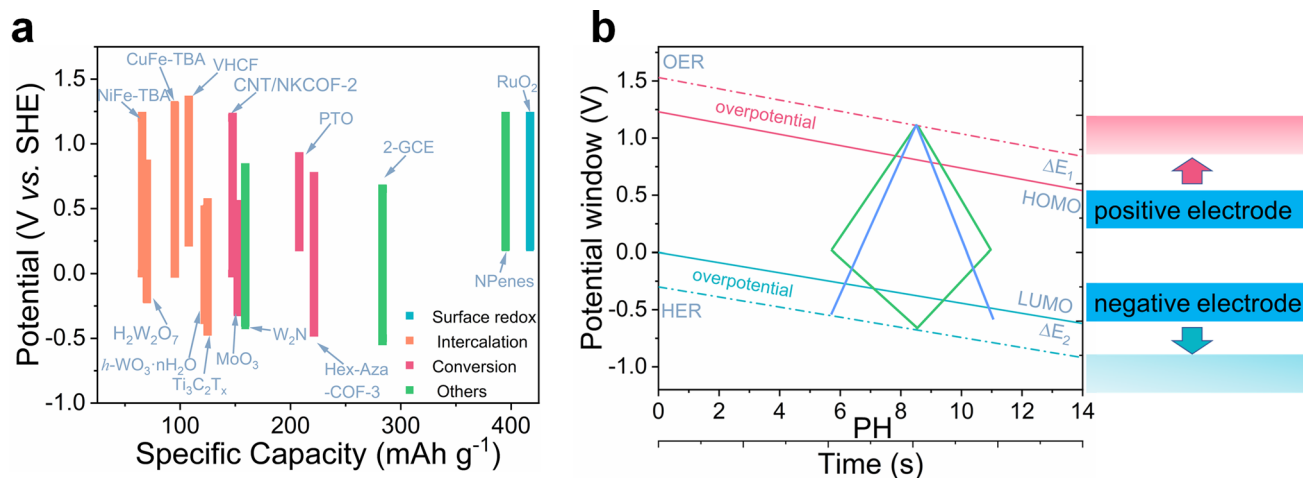
Fig. 9 **a** Summary of the potential window of various electrode materials for EPS. **b** Schematic of potential window of a water-based full cell at different PH

and charge storage mechanism of organic electrodes needs to be further explored. Lots of reported electrode materials for electrochemical proton storage are summarized in Table 1.

4 Device Configuration

The goal of the research on materials and charge storage mechanisms of electrochemical proton storage is to develop more efficient batteries/capacitors and lead the
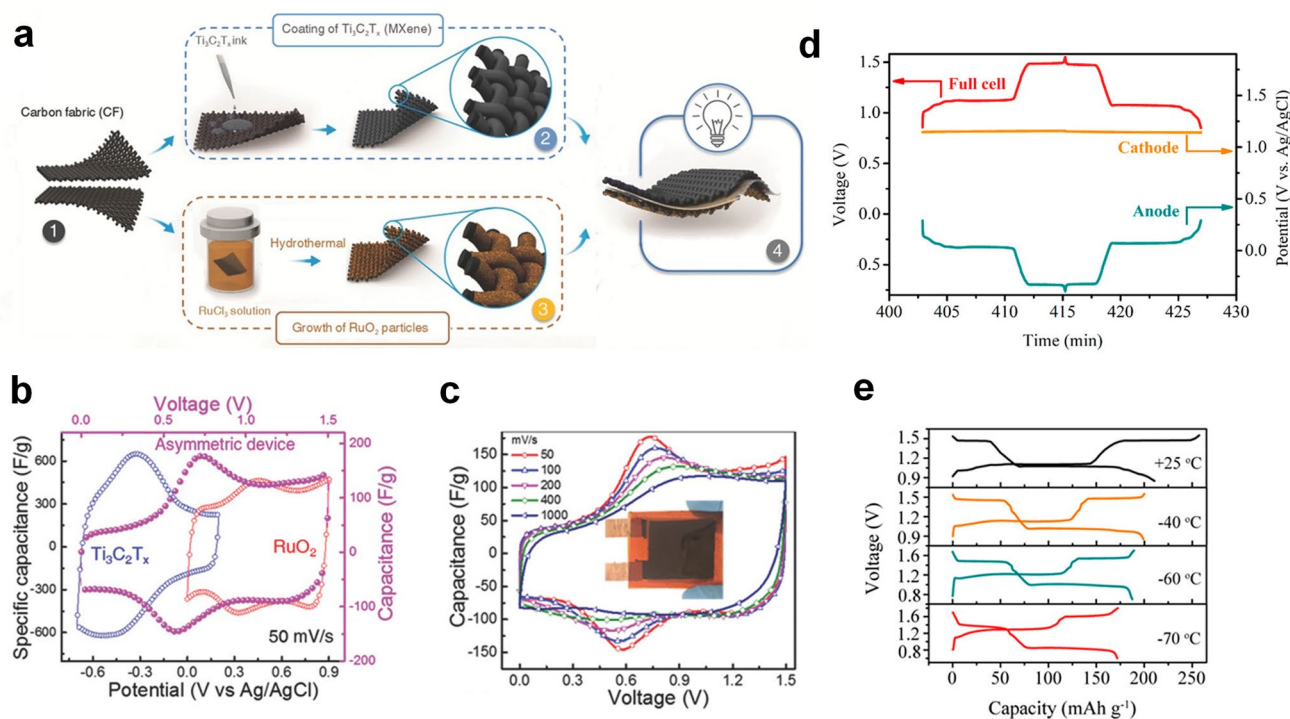
Fig. 10 **a** The fabrication process of $RuO_2//Ti_3C_2T_x$ asymmetric proton pseudocapacitor. **b** In situ tracked variation of the potential in RuO_2/CF electrode, $Ti_3C_2T_x/CF$ electrode, and $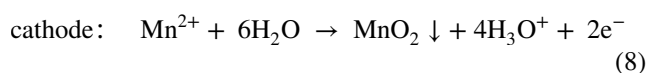RuO_2//Ti_3C_2T_x$ asymmetric device. **c** Capacitance of $RuO_2//Ti_3C_2T_x$ asymmetric device at different scan rates [103]. Copyright 2018, Wiley–VCH. **d** The comparison of galvanostatic charge–discharge curves of $MnO_2@GF//MoO_3$ full cell, $MnO_2@GF$ cathode, and MoO_3 anode at 1 mA cm^{-2}. **e** Galvanostatic charge–discharge curves of $MnO_2@GF//MoO_3$ full cell at different temperatures [40]. Copyright 2020, American Chemical Society

way to its industrialization. To achieve the above goals, it is very necessary to build a complete full cell device (Fig. 9a–b). Jiang et al. designed an all pseudocapacitive asymmetric supercapacitor using MXene ($Ti_3C_2T_x$) as the negative electrode and ruthenium oxide (RuO_2) as the positive electrode (Fig. 10a) [103]. This asymmetric supercapacitor operated at a voltage of 1.5 V in 1 M H_2SO_4, which far surpassed other MXene-based supercapacitors (Fig. 10b). More importantly, this supercapacitor exhibited extraordinary rate performance with a capacity retention of 84% at a high scan rate of 1000 mV s^{-1} (relative to the specific capacitance at 50 mV s^{-1}), resulting in that the asymmetric device delivered an energy density of 24 Wh kg^{-1} at a power density of 26 kW kg^{-1} (Fig. 10c). Boota et al. demonstrated some working asymmetric proton pseudocapacitors using MXene ($Ti_3C_2T_x$) as the negative electrode and conducting polymers (PANI@rGO, PPy@rGO, and PEDOT@rGO) as the positive electrode [104]. Owing to the complementary electrochemical window of positive and negative materials and the pseudocapacitive reaction

derived from protons, the voltage window of these all pseudocapacitors reached 1.45 V in 3 M H_2SO_4. Moreover, the presence of rGO not only increased the conductivity of CPs but also improved the cycle stability of electrodes, and the asymmetric device of PANI@rGO//$Ti_3C_2T_x$ showed capacitance retention of $\approx$ 88% after 20,000 cycles. Therefore, the composite electrode is a strategy that can be considered in the construction of a full cell, especially in improving the cycle stability of a device. An organic–inorganic all-pseudocapacitive supercapacitor with a MXene anode and a 2,5-dihydroxy-1,4-benzoquinone (DBQ)@ rGO cathode was also investigated by Boota et al. [105]. Recently, our group reported an all proton pseudocapacitor with a Prussian analog ($Cu_{0.82}Co_{0.18}HCF$) as cathode and $WO_3 \cdot nH_2O$ as anode with a voltage of 1.7 V, which delivered an energy density of 22 Wh kg^{-1} at a high power density of 26 kW kg^{-1} [106].

Jiang et al. designed a full proton battery using H-TBA as cathode, MoO_3 as the anode, and 9.5 M H_3PO_4 as the electrolyte, which delivered a high capacity of 46 mAh g^{-1}

at 5 A g^{-1} and capacity retention of 70% at100 A g^{-1}. 9.5 M H$_3$PO$_4$ with a freezing point of below −88 °C enabled this full proton battery to exhibit a specific capacity of 28 mAh g^{-1} and specific energy density of 24 Wh kg^{-1} at an ultra-low temperature of −78 ℃. With the discovery of the co-intercalation mechanism of protons and metal ions in many materials (such as MnO$_2$ and V$_2$O$_5$) [107, 108], some multi-ion batteries have been developed. Yan et al. developed a full cell using MoO$_3$ as the anode and MnO$_2$ as the cathode in a mixed electrolyte (2 M H$_2$SO$_4$ + 2 M MnSO$_4$) (Fig. 10d) [40]. Therefore, the following reactions occurred in cathode and anode:

$$\text{cathode：} \quad Mn^{2+} + 6H_2O \rightarrow MnO_2 \downarrow + 4H_3O^+ + 2e^- \tag{8}$$

$$\text{anode：} \quad xH_3O^+ + xe^- + MoO_3 \rightarrow (H_3O)_x MoO_3 \tag{9}$$

Then, the MnO$_2$@GF//MoO$_3$ full cell with a 1.6 V voltage window achieved a maximum energy density of 177.4 Wh kg^{-1} at a power density of 895.9 W kg^{-1}, which was the highest energy density reported to date for a proton full cell (Fig. 10d). In particular, the acid solution with high conductivity not only increased the ioni c conductivity of the mixed electrolyte but also significantly reduced the freezing point of the mixed electrolyte. Finally, this full cell still possessed a specific capacity of 171.8 mAh g^{-1} at an ultralow low temperature of − 70 °C and cycled for 100 cycles without capacity fading (Fig. 10e). A similar full cell with a MnO$_2$@graphite felt cathode and a pyrene-4,5,9,10-tetraone (PTO) anode was also reported by Guo et al. [33]. Similarly, this organic/inorganic full cell had excellent electrochemical performance (energy density of 132.6 Wh kg^{-1}) and low-temperature performance (nearly 72% of the room-temperature capacity at −70 °C). This strategy of proton–metal ion hybrid full cell efficiently takes advantage of the high energy of metal ion batteries and high power of proton batteries and provides a new avenue for the construction of proton full cell. A very novel proton–gas battery with an H$_2$ anode electrode, CuHCF cathode electrode, and 9 M H$_3$PO$_4$ electrolyte was also developed, which delivered a long cycle life over 0.35 million cycles [109]. More importantly, this CuHCF–H$_2$ cell achieved an outstanding rate capacity of 30 mAh g^{-1} and cycled steadily over 1150 cycles at −60 °C. Some manganese–hydrogen batteries and nickel–hydrogen batteries with high energy, long life, and low cost have been successfully produced commercially for large-scale energy storage. Proton electrochemical energy storage devices not only achieve high energy density and power density but also show outstanding application value at extremely low temperatures [110, 111].

5 Summary and Outlook

The development of energy internet and energy revolution technology is pushing for the application of electrochemical energy storage (EES) in various industries, and EPS will occupy an important place in the development of energy. Compared with traditional metal ion charge carrier batteries or capacitors, proton batteries and pseudocapacitors have been extensively studied for combined advantages of high capacity, superior rate, and long life in recent years. Specifically, this review systematically summarizes and discusses the preparation technology, electrochemical performance, and charge storage mechanism for the existing proton battery-type/ pseudocapacitive materials. According to different charge storage mechanisms, it is mainly classified into surface redox type, intercalation type, and conversion type. Although some progress has been made in proton electrochemical energy storage, it is still a key challenge to develop electrode materials for electrochemical proton storage with excellent performance, low cost, and high safety. Then, we also summarized the progress of the construction of EPS devices in detail, which enlightened significance for our understanding of this new type of energy storage system. Therefore, there is still more work that needs to be done to thoroughly understand the basic mechanisms of electrochemical proton storage and to build superior energy storage systems.

5.1 Mechanism Understanding of EPS

The solid-phase reaction stage of common lithium-ion batteries is a typical diffusion-controlled process with a time scale of a few minutes, which makes it difficult to increase the power density of the lithium-ion batteries. In recent years, the vigorous development of the energy storage industry has increased the demand for power batteries, increasing people's interest in exploring electrode materials with high diffusion coefficients. Although proton battery-type/pseudocapacitive materials undergo an intercalation/conversion reaction similar to the battery during charge and discharge, most of them are nondiffusion-controlled on the time scale, so most of them can be considered as pseudocapacitive in nature. Furthermore, proton battery-type/pseudocapacitive materials seem to be a potential opportunity that achieves

high power density and energy density because it combines the advantages of batteries and capacitors. However, there is still unclear as to why protons are transported so rapidly in these electrode materials. Though some people thought that protons could be rapidly transported on the hydrogen bond network through the Grotthuss diffusion mechanism, there was no direct evidence so far. The key parameters such as the physical and chemical properties of protons, interface effects, and energy changes will be effectively combined through theoretical calculations, and using cutting-edge theory establishes a reasonable structural model from the atomic scale to understand the charge storage mechanisms of EPS. Advanced in situ characterization techniques are also indispensable for tracing transport pathways of protons and revealing binding sites of protons and electrode materials during proton storage. The determination of the interaction between electrode materials and protons will be of significance for the design of advanced proton battery-type/pseudocapacitive materials.

5.2 Electrode Design of EPS

Electrode materials are of paramount importance to improving the electrochemical performance of EPS. The anode material with a higher overpotential that is conducive to reducing hydrogen evolution reaction (HER) is a suitable host for proton storage [112]; current anode materials are concentrated on W-based, Mo-based, and Ti-based electrode materials in the light of Trassati's volcano plot [113]. More anode materials with high-capacity, high-rate performance, and cyclic stability can be developed through designing rational lattice structures and regulating structural waters to build a continuous hydrogen bond network. Additionally, greater efforts are needed to design efficient high-voltage-resistant cathode materials because there is that only Prussian blue analogue cathode materials deliver good electrochemical performance. Polyanionic compounds (such as $VOPO_4$) with high theoretical capacity and theoretical redox potential have been designed as electrode materials for lithium-ion batteries, which are also promising high-voltage cathode materials for EPS. On the one hand, it is important to understand the influence of defect structure on electrochemical performance, which may help us optimize synthesis methods to add more active sites to store more

protons. On the other hand, water molecules (including free water and structural water) and surface functional groups in electrode materials have a significant impact on their electrochemical performance. Reasonable defect distribution and appropriate water content/surface groups will facilitate the building of a complete hydrogen bond network, which may be a highway for rapid proton transport. Therefore, it is crucial to explore safe, reliable, and low-cost routes to prepare more controlled electrode materials with high capacity and wide potential (especially high-voltage cathode materials).

5.3 Device Configuration of EPS

The current application research on EPS is mainly concentrated in acidic aqueous solution, so that proton batteries/pseudocapacitors deliver a low energy density owing to the decomposition of water under a lower voltage. The research focus of EPS can be appropriately shifted to the development of electrolytes with a wide electrochemical window, such as aqueous hybrid electrolytes (additive, water-organic, etc.), organic acids, and proton ionic liquids for their large decomposition voltage windows [114]. Recently, some work on widening the electrochemical windows of aqueous electrolytes has been reported [115, 116]. For example, adding some sodium dodecyl sulfate (SDS) electrolyte to water led the voltage window to expand to 2.5 V because of the reason that the hydrophobic layer formed by SDS electrostatically adsorbed to the electrode surface and effectively prevented the generation of OER/HER [116]. How to optimize aqueous electrolytes preparation or regulate high-efficiency organic protonic electrolytes and explore the mechanism and dynamics of electrochemical proton storage are awaiting further research. Moreover, another effective way to increase operating voltage is to build full-cell configurations and maintain a good charge balance, which can make full use of the positive and negative voltage windows, which has been confirmed to be the easiest way to expand the operating voltage of electronic double-layer capacitors and pseudocapacitors [117]. It is also a good way to develop proton-metal ion hybrid batteries to maximize energy and power density by combining the rapid kinetics of protons with the high energy of metal ions. More matching strategies of positive and negative electrodes need to be further explored, which is i mportant to the development of

electrochemical proton storage devices with high specific energy and power.

5.4 Practical Application of EPS

To meet the demand for grid-scale energy storage, the practical application of EPS devices must be developed. Proton batteries and pseudocapacitors have advantages of simultaneously maximizing energy density and power density, to bridge the gap between metal-ion batteries and capacitors. Proton batteries/capacitors will occupy some special markets in the future. The fast kinetics of proton electrochemical energy storage not only endow proton batteries/capacitors with higher rate characteristics compared to metal-ion batteries, but also the potential to operate at ultra-low temperatures. On the one hand, freezing points of electrolytes generally will be lowered by using acidic electrolytes rich in protons (such as "water-in-acid" electrolytes). On the other hand, protons can be transported inside the lattice via the Grotthuss mechanism (over 60% capacity retention below –60 ℃ for many proton batteries/capacitors), while the transport speed of metal ions in liquid and solid states decreases significantly with decreasing temperature (~ 10% capacity retention at –40 ℃ for LIBs). Further electrolyte optimization and electrode material structure design will facilitate the practical application of EPS in harsh environments such as polar, aerospace, and military weapons. Besides, the development of the connected and smart environment will promote the applications of EPS in such an emerging application field; therefore, it is very necessary to build compact, efficient, and miniaturized micro-scale energy storage devices for EPS [19]. To meet the needs of flexible and wearable technology, the structural design of proton batteries and pseudocapacitors must be combined with advanced technologies such as laser-based techniques and 3D printing to build better proton micro-batteries/micro-supercapacitors.

References

1. B. Dunn, H. Kamath, J.M. Tarascon, Electrical energy storage for the grid: a battery of choices. Science **334**(6058), 928–935 (2011). https://doi.org/10.1126/science.1212741

2. Y. Gogotsi, P. Simon, True performance metrics in electrochemical energy storage. Science **334**(6058), 917–918 (2011). https://doi.org/10.1126/science.1213003

3. Z. Li, B.Y. Guan, J.T. Zhang, X.W. Lou, A compact nanoconfined sulfur cathode for high-performance lithium-sulfur batteries. Joule **1**(3), 576–587 (2017). https://doi.org/10.1016/j.joule.2017.06.003

4. Y.J. Liu, X.Y. Tao, Y. Wang, C. Jiang, C. Ma et al., Self-assembled monolayers direct a LiF-rich interphase toward long-life lithium metal batteries. Science **375**(6582), 739–745 (2022). https://doi.org/10.1126/science.abn1818

5. D.Q. Cao, X.X. Shen, A.P. Wang, F.J. Yu, Y.P. Wu et al., Threshold potentials for fast kinetics during mediated redox catalysis of insulators in Li-O$_2$ and Li-S batteries. Nat. Catal. **5**, 193–201 (2022). https://doi.org/10.1038/s41929-022-00752-z

6. X. Gao, Y. Chen, L.R. Johnson, Z.P. Jovanov, P.G. Bruce, A rechargeable lithium-oxygen battery with dual mediators stabilizing the carbon cathode. Nat. Energy **2**(9), 17118 (2017). https://doi.org/10.1038/nenergy.2017.118

7. D. Wang, J. Yang, P. He, H. Zhou, A low-charge-overpotential lithium-CO$_2$ cell based on a binary molten salt electrolyte. Energy Environ. Sci. **14**(7), 4107–4114 (2021). https://doi.org/10.1039/d1ee00068c

8. K. Baek, W.C. Jeon, S. Woo, J.C. Kim, J.G. Lee et al., Synergistic effect of quinary molten salts and ruthenium catalyst for high-power-density lithium-carbon dioxide cell. Nat. Commun. **11**, 456 (2020). https://doi.org/10.1038/s41467-019-14121-1

9. E. Fan, L. Li, Z. Wang, J. Lin, Y. Huang et al., Sustainable recycling technology for Li-ion batteries and beyond: challenges and future prospects. Chem. Rev. **120**(14), 7020–7063 (2020). https://doi.org/10.1021/acs.chemrev.9b00535

10. C. Delmas, Sodium and sodium-ion batteries: 50 years of research. Adv. Energy Mater. **8**(17), 1703137 (2018). https://doi.org/10.1002/aenm.201703137

11. T. Hosaka, K. Kubota, A.S. Hameed, S. Komaba, Research development on K-ion batteries. Chem. Rev. **120**(14), 6358–6466 (2020). https://doi.org/10.1021/acs.chemrev.9b00463

12. C. Zhong, B. Liu, J. Ding, X. Liu, Y. Zhong et al., Decoupling electrolytes towards stable and high-energy rechargeable aqueous zinc-manganese dioxide batteries. Nat. Energy **5**(6), 440–449 (2020). https://doi.org/10.1038/s41560-020-0584-y

13. A. Du, Z. Zhang, H. Qu, Z. Cui, L. Qiao et al., An efficient organic magnesium borate-based electrolyte with non-nucleophilic characteristics for magnesium-sulfur battery. Energy Environ. Sci. **10**(12), 2616–2625 (2017). https://doi.org/10.1039/c7ee02304a

14. M.C. Lin, M. Gong, B. Lu, Y. Wu, D.Y. Wang et al., An ultrafast rechargeable aluminium-ion battery. Nature **520**(7547), 325–328 (2015). https://doi.org/10.1038/nature14340

15. S. Dong, W. Shin, H. Jiang, X. Wu, Z. Li et al., Ultra-fast NH_4^+ storage: strong H bonding between NH_4^+ and bi-layered V_2O_5. Chem **5**(6), 1537–1551 (2019). https://doi.org/10.1016/j.chempr.2019.03.009

16. G. Liang, Y. Wang, Z. Huang, F. Mo, X. Li et al., Initiating hexagonal MoO_3 for superb-stable and fast NH_4^+ storage based on hydrogen bond chemistry. Adv. Mater. **32**(14), 1907802 (2020). https://doi.org/10.1002/adma.201907802

17. X. Wu, Y. Qi, J.J. Hong, Z. Li, A.S. Hernandez et al., Rocking-chair ammonium-ion battery: a highly reversible aqueous energy storage system. Angew. Chem. Int. Ed. **56**(42), 13026–13030 (2017). https://doi.org/10.1002/anie.201707473

18. M. Salanne, B. Rotenberg, K. Naoi, K. Kaneko, P.L. Taberna et al., Efficient storage mechanisms for building better supercapacitors. Nat. Energy **1**(6), 16070 (2016). https://doi.org/10.1038/nenergy.2016.70

19. P. Simon, Y. Gogotsi, Perspectives for electrochemical capacitors and related devices. Nat. Mater. **19**(11), 1151–1163 (2020). https://doi.org/10.1038/s41563-020-0747-z

20. Y. Xu, X. Wu, X. Ji, The renaissance of proton batteries. Small Struct. **2**(5), 2000113 (2021). https://doi.org/10.1002/sstr.202000113

21. X. Wu, J.J. Hong, W. Shin, L. Ma, T. Liu et al., Diffusion-free Grotthuss topochemistry for high-rate and long-life proton batteries. Nat. Energy **4**(2), 123–130 (2019). https://doi.org/10.1038/s41560-018-0309-7

22. C. Knight, G.A. Voth, The curious case of the hydrated proton. Acc. Chem. Res. **45**(1), 101–109 (2012). https://doi.org/10.1021/ar200140h

23. C.T. Wolke, J.A. Fournier, L.C. Dzugan, M.R. Fagiani, T.T. Odbadrakh et al., Spectroscopic snapshots of the proton-transfer mechanism in water. Science **354**(6316), 1131–1135 (2016). https://doi.org/10.1126/science.aaf8425

24. S.M.S.E. Adabifiroozjaei, Y. Yao, P. Koshy, S. Lim, R. Webster et al., Proton-assisted creation of controllable volumetric oxygen vacancies in ultrathin CeO_{2-x} for pseudo-capacitive energy storage applications. Nat. Commun. **10**, 2594 (2019). https://doi.org/10.1038/s41467-019-10621-2

25. D.W. Lim, M. Sadakiyo, H. Kitagawa, Proton transfer in hydrogen-bonded degenerate systems of water and ammonia in metal-organic frameworks. Chem. Sci. **10**(1), 16–33 (2019). https://doi.org/10.1039/c8sc04475a

26. Z. Chen, Y. Peng, F. Liu, Z. Le, J. Zhu et al., Hierarchical nanostructured WO_3 with biomimetic proton channels and mixed ionic-electronic conductivity for electrochemical energy storage. Nano Lett. **15**(10), 6802–6808 (2015). https://doi.org/10.1021/acs.nanolett.5b02642

27. M.R. Lukatskaya, S. Kota, Z. Lin, M.Q. Zhao, N. Shpigel et al., Ultra-high-rate pseudocapacitive energy storage in two-dimensional transition metal carbides. Nat. Energy **2**(8), 17105 (2017). https://doi.org/10.1038/nenergy.2017.105

28. X. Wang, Y. Xie, K. Tang, C. Wang, C. Yan, Redox chemistry of molybdenum trioxide for ultrafast hydrogen-ion storage. Angew. Chem. Int. Ed. **57**(36), 11569–11573 (2018). https://doi.org/10.1002/anie.201803664

29. D.P. Dubal, N.R. Chodankar, S. Qiao, Tungsten nitride nanodots embedded phosphorous modified carbon fabric as flexible and robust electrode for asymmetric pseudocapacitor. Small **15**(1), 1804104 (2019). https://doi.org/10.1002/smll.201804104

30. Z. Wu, L. Jiang, W. Tian, Y. Wang, Y. Jiang et al., Novel sub-5 nm layered niobium phosphate nanosheets for high-voltage, cation-intercalation typed electrochemical energy storage in wearable pseudocapacitors. Adv. Energy Mater. **9**(20), 1900111 (2019). https://doi.org/10.1002/aenm.201900111

31. G. Liang, F. Mo, X. Ji, C. Zhi, Non-metallic charge carriers for aqueous batteries. Nat. Rev. Mater. **6**(2), 109–123 (2020). https://doi.org/10.1038/s41578-020-00241-4

32. D.L. Chao, W.H. Zhou, F.X. Xie, C. Ye, H. Li et al., Roadmap for advanced aqueous batteries: from design of materials to applications. Sci. Adv. **6**(21), eaba4098 (2020). https://doi.org/10.1126/sciadv.aba4098

33. Z. Guo, J. Huang, X. Dong, Y. Xia, L. Yan et al., An organic/inorganic electrode-based hydronium-ion battery. Nat. Commun. **11**, 959 (2020). https://doi.org/10.1038/s41467-020-14748-5

34. J. Huang, S. Peng, J. Gu, G. Chen, J. Gao et al., Self-powered integrated system of a strain sensor and flexible all-solid-state supercapacitor by using a high performance ionic organohydrogel. Mater. Horiz. **7**(8), 2085–2096 (2020). https://doi.org/10.1039/d0mh00100g

35. H. Jiang, W. Shin, L. Ma, J.J. Hong, Z. Wei et al., A high-rate aqueous proton battery delivering power below − 78 °C via an unfrozen phosphoric acid. Adv. Energy Mater. **10**(28), 2000968 (2020). https://doi.org/10.1002/aenm.202000968

36. C. Lu, X. Chen, All-temperature flexible supercapacitors enabled by antifreezing and thermally stable hydrogel electrolyte. Nano Lett. **20**(3), 1907–1914 (2020). https://doi.org/10.1021/acs.nanolett.9b05148

37. C. Strietzel, M. Sterby, H. Huang, M. Stromme, R. Emanuelsson et al., An aqueous conducting redox-polymer-based proton battery that can withstand rapid constant-voltage charging

and sub-zero temperatures. Angew. Chem. Int. Ed. **59**(24), 9631–9638 (2020). https://doi.org/10.1002/anie.202001191

38. X. Wu, S. Qiu, Y. Xu, L. Ma, X. Bi et al., Hydrous nickel-iron turnbull's blue as a high-rate and low-temperature proton electrode. ACS Appl. Mater. Interfaces **12**(8), 9201–9208 (2020). https://doi.org/10.1021/acsami.9b20320

39. J. Xu, X. Hu, X. Wang, X. Wang, Y. Ju et al., Low-temperature pseudocapacitive energy storage in $Ti_3C_2T_x$ MXene. Energy Stor. Mater. **33**, 382–389 (2020). https://doi.org/10.1016/j.ensm.2020.08.029

40. L. Yan, J. Huang, Z. Guo, X. Dong, Z. Wang et al., Solid-state proton battery operated at ultralow temperature. ACS Energy Lett. **5**(2), 685–691 (2020). https://doi.org/10.1021/acsenergylett.0c00109

41. C. Choi, D.S. Ashby, D.M. Butts, R.H. DeBlock, Q. Wei et al., Achieving high energy density and high power density with pseudocapacitive materials. Nat. Rev. Mater. **5**, 5–19 (2019). https://doi.org/10.1038/s41578-019-0142-z

42. F. Liu, T. Wang, X. Liu, L.Z. Fan, Challenges and recent progress on key materials for rechargeable magnesium batteries. Adv. Energy Mater. **11**(2), 2000787 (2020). https://doi.org/10.1002/aenm.202000787

43. J.P. Zheng, P.J. Cygan, T.R. Jow, Hydrous ruthenium oxide as an electrode material for electrochemical capacitors. J. Electrochem. Soc. **142**(8), 2699–2703 (1995). https://doi.org/10.1149/1.2050077

44. W. Dmowski, T. Egami, K.E. Swider-Lyons, C.T. Love, D.R. Rolison, Local atomic structure and conduction mechanism of nanocrystalline hydrous RuO_2 from X-ray scattering. J. Phys. Chem. B **106**(49), 12677–12683 (2002). https://doi.org/10.1021/jp026228l

45. N. Yoshida, Y. Yamada, S. Nishimura, Y. Oba, M. Ohnuma et al., Unveiling the origin of unusual pseudocapacitance of $RuO_2 \cdot nH_2O$ from its hierarchical nanostructure by small-angle X-ray scattering. J. Phys. Chem. C **117**(23), 12003–12009 (2013). https://doi.org/10.1021/jp403402k

46. V. Ozolins, F. Zhou, M. Asta, Ruthenia-based electrochemical supercapacitors: insights from first-principles calculations. Acc. Chem. Res. **46**(5), 1084–1093 (2013). https://doi.org/10.1021/ar3002987

47. Y. Liu, F. Zhou, V. Ozolins, Ab initio study of the charge-storage mechanisms in RuO_2-based electrochemical ultracapacitors. J. Phys. Chem. C **116**(1), 1450–1457 (2011). https://doi.org/10.1021/jp207616s

48. C. Costentin, T.R. Porter, J.M. Saveant, How do pseudocapacitors store energy? Theoretical analysis and experimental illustration. ACS Appl. Mater. Interfaces **9**(10), 8649–8658 (2017). https://doi.org/10.1021/acsami.6b14100

49. A. Jadon, S. Prabhudev, G. Buvat, S.G. Patnaik, M. Djafari-Rouhani et al., Rethinking pseudocapacitance: a way to harness charge storage of crystalline RuO_2. ACS Appl. Energy Mater. **3**(5), 4144–4148 (2020). https://doi.org/10.1021/acsaem.0c00476

50. H.A. Evans, Y. Wu, R. Seshadri, A.K. Cheetham, Perovskite-related ReO_3-type structures. Nat. Rev. Mater. **5**(3), 196–213 (2020). https://doi.org/10.1038/s41578-019-0160-x

51. S. Tanisaki, Crystal structure of monoclinic tungsten trioxide at room temperature. J. Phys. Soc. Jpn. **15**(4), 573–581 (1960). https://doi.org/10.1143/JPSJ.15.573

52. S.H. Lee, R. Deshpande, P.A. Parilla, K.M. Jones, B. To et al., Crystalline WO_3 nanoparticles for highly improved electrochromic applications. Adv. Mater. **18**(6), 763–766 (2006). https://doi.org/10.1002/adma.200501953

53. J.D.E. McIntyre, S. Basu, W.F. Peck, W.L. Brown, W.M. Augustyniak, Cation insertion reactions of electrochromic tungsten and iridium oxide films. Phys. Rev. B **25**(12), 7242–7254 (1982). https://doi.org/10.1103/PhysRevB.25.7242

54. P.G. Dickens, S. Crouch-Baker, M.T. Weller, Hydrogen insertion in oxides. Solid State Ion. **18–19**, 89–97 (1986). https://doi.org/10.1016/0167-2738(86)90092-5

55. S.J. Babinec, A quartz crystal microbalance analysis of ion insertion into WO_3. Sol. Energy Mater Sol. Cells **25**(3–4), 269–291 (1992). https://doi.org/10.1016/0927-0248(92)90073-x

56. M.S. Whittingham, Hydrogen motion in oxides: from insulators to bronzes. Solid State Ion. **168**(3–4), 255–263 (2004). https://doi.org/10.1016/j.ssi.2003.08.056

57. M. Zhu, W. Meng, Y. Huang, Y. Huang, C. Zhi, Proton-insertion-enhanced pseudocapacitance based on the assembly structure of tungsten oxide. ACS Appl. Mater. Interfaces **6**(21), 18901–18910 (2014). https://doi.org/10.1021/am504756u

58. J.B. Mitchell, W.C. Lo, A. Genc, J. LeBeau, V. Augustyn, Transition from battery to pseudocapacitor behavior via structural water in tungsten oxide. Chem. Mater. **29**(9), 3928–3937 (2017). https://doi.org/10.1021/acs.chemmater.6b05485

59. J. Besnardiere, B. Ma, A. Torres-Pardo, G. Wallez, H. Kabbour et al., Structure and electrochromism of two-dimensional octahedral molecular sieve h'-WO_3. Nat. Commun. **10**, 327 (2019). https://doi.org/10.1038/s41467-018-07774-x

60. W. Sun, M.T. Yeung, A.T. Lech, C.W. Lin, C. Lee et al., High surface area tunnels in hexagonal WO_3. Nano Lett. **15**(7), 4834–4838 (2015). https://doi.org/10.1021/acs.nanolett.5b02013

61. M. Zhu, Y. Huang, Y. Huang, Z. Pei, Q. Xue et al., Capacitance enhancement in a semiconductor nanostructure-based supercapacitor by solar light and a self-powered supercapacitor-photodetector system. Adv. Funct. Mater. **26**(25), 4481–4490 (2016). https://doi.org/10.1002/adfm.201601260

62. E.V. Miu, J.R. McKone, Comparisons of WO_3 reduction to H_xWO_3 under thermochemical and electrochemical control. J. Mater. Chem. A **7**(41), 23756–23761 (2019). https://doi.org/10.1039/c9ta06394c

63. H. Jiang, J.J. Hong, X. Wu, T.W. Surta, Y. Qi et al., Insights on the proton insertion mechanism in the electrode of hexagonal tungsten oxide hydrate. J. Am. Chem. Soc. **140**(37), 11556–11559 (2018). https://doi.org/10.1021/jacs.8b03959

64. A. Hu, Z. Jiang, C. Kuai, S. McGuigan, D. Nordlund et al., Uncovering phase transformation, morphological evolution, and nanoscale color heterogeneity in tungsten oxide

electrochromic materials. J. Mater. Chem. A **8**(38), 20000–20010 (2020). https://doi.org/10.1039/d0ta06612e

65. H. Lin, F. Zhou, C.P. Liu, V. Ozoliņš, Non-grotthuss proton diffusion mechanism in tungsten oxide dihydrate from first-principles calculations. J. Mater. Chem. A **2**(31), 12280–12288 (2014). https://doi.org/10.1039/c4ta02465f

66. R. Wang, J.B. Mitchell, Q. Gao, W.Y. Tsai, S. Boyd et al., Operando atomic force microscopy reveals mechanics of structural water driven battery-to-pseudocapacitor transition. ACS Nano **12**(6), 6032–6039 (2018). https://doi.org/10.1021/acsnano.8b02273

67. J.B. Mitchell, N.R. Geise, A.R. Paterson, N.C. Osti, Y. Sun et al., Confined interlayer water promotes structural stability for high-rate electrochemical proton intercalation in tungsten oxide hydrates. ACS Energy Lett. **4**(12), 2805–2812 (2019). https://doi.org/10.1021/acsenergylett.9b02040

68. A. Zhou, W. Cheng, W. Wang, Q. Zhao, J. Xie et al., Hexacyanoferrate-type Prussian blue analogs: principles and advances toward high-performance sodium and potassium ion batteries. Adv. Energy Mater. **11**(2), 2000943 (2020). https://doi.org/10.1002/aenm.202000943

69. A. Simonov, T.D. Baerdemaeker, H.L.B. Bostrom, M.L.R. Gomez, H.J. Gray et al., Hidden diversity of vacancy networks in Prussian blue analogues. Nature **578**(7794), 256–260 (2020). https://doi.org/10.1038/s41586-020-1980-y

70. X. He, L. Tian, M. Qiao, J. Zhang, W. Geng et al., A novel highly crystalline $Fe_4(Fe(CN)_6)_3$ concave cube anode material for Li-ion batteries with high capacity and long life. J. Mater. Chem. A **7**(18), 11478–11486 (2019). https://doi.org/10.1039/c9ta02265a

71. L. Jiang, Y. Lu, C. Zhao, L. Liu, J. Zhang et al., Building aqueous K-ion batteries for energy storage. Nat. Energy **4**(6), 495–503 (2019). https://doi.org/10.1038/s41560-019-0388-0

72. J.H. Lee, G. Ali, D.H. Kim, K.Y. Chung, Metal-organic framework cathodes based on a vanadium hexacyanoferrate Prussian blue analogue for high-performance aqueous rechargeable batteries. Adv. Energy Mater. **7**(2), 1601491 (2017). https://doi.org/10.1002/aenm.201601491

73. Z. Li, K. Xiang, W. Xing, W.C. Carter, Y.M. Chiang, Reversible aluminum-ion intercalation in Prussian blue analogs and demonstration of a high-power aluminum-ion asymmetric capacitor. Adv. Energy Mater. **5**(5), 1401410 (2015). https://doi.org/10.1002/aenm.201401410

74. L. Ma, S. Chen, C. Long, X. Li, Y. Zhao et al., Achieving high-voltage and high-capacity aqueous rechargeable zinc ion battery by incorporating two-species redox reaction. Adv. Energy Mater. **9**(45), 1902446 (2019). https://doi.org/10.1002/aenm.201902446

75. X. Peng, H. Guo, W. Ren, Z. Su, C. Zhao, Vanadium hexacyanoferrate as high-capacity cathode for fast proton storage. Chem. Commun. **56**(79), 11803–11806 (2020). https://doi.org/10.1039/d0cc03974h

76. K. Ono, M. Ishizaki, K. Kanaizuka, T. Togashi, T. Yamada et al., Grain-boundary-free super-proton conduction of a solution-processed prussian-blue nanoparticle film. Angew.

Chem. Int. Ed. **56**(20), 5531–5535 (2017). https://doi.org/10.1002/anie.201701759

77. S. Ohkoshi, K. Nakagawa, K. Tomono, K. Imoto, Y. Tsunobuchi et al., High proton conductivity in Prussian blue analogues and the interference effect by magnetic ordering. J. Am. Chem. Soc. **132**(19), 6620–6621 (2010). https://doi.org/10.1021/ja100385f

78. P. Higel, F. Villain, M. Verdaguer, E. Riviere, A. Bleuzen, Solid-state magnetic switching triggered by proton-coupled electron-transfer assisted by long-distance proton-alkali cation transport. J. Am. Chem. Soc. **136**(17), 6231–6234 (2014). https://doi.org/10.1021/ja502294x

79. M. Naguib, M. Kurtoglu, V. Presser, J. Lu, J. Niu et al., Two-dimensional nanocrystals produced by exfoliation of Ti_3AlC_2. Adv. Mater. **23**(37), 4248–4253 (2011). https://doi.org/10.1002/adma.201102306

80. Y.T. Liu, P. Zhang, N. Sun, B. Anasori, Q.Z. Zhu et al., Self-assembly of transition metal oxide nanostructures on MXene nanosheets for fast and stable lithium storage. Adv. Mater. **30**(23), 1707334 (2018). https://doi.org/10.1002/adma.201707334

81. Z. Lin, D. Barbara, P.L. Taberna, K.L.V. Aken, B. Anasori et al., Capacitance of $Ti_3C_2T_x$ MXene in ionic liquid electrolyte. J. Power Sources **326**, 575–579 (2016). https://doi.org/10.1016/j.jpowsour.2016.04.035

82. J. Yu, J. Zhou, P. Yao, H. Xie, M. Zhang et al., Antimonene engineered highly deformable freestanding electrode with extraordinarily improved energy storage performance. Adv. Energy Mater. **9**(44), 1902462 (2019). https://doi.org/10.1002/aenm.201902462

83. M.R. Lukatskaya, S.M. Bak, X. Yu, X.Q. Yang, M.W. Barsoum et al., Probing the mechanism of high capacitance in 2D titanium carbide using in situ X-ray absorption spectroscopy. Adv. Energy Mater. **5**(15), 1500589 (2015). https://doi.org/10.1002/aenm.201500589

84. M.R. Lukatskaya, O. Mashtalir, C.E. Ren, Y. Dall'Agnese, P. Rozier et al., Cation intercalation and high volumetric capacitance of two-dimensional titanium carbide. Science **341**(6153), 1502–1505 (2013). https://doi.org/10.1126/science.1241488

85. X. Mu, D. Wang, F. Du, G. Chen, C. Wang et al., Revealing the pseudo-intercalation charge storage mechanism of MXenes in acidic electrolyte. Adv. Funct. Mater. **29**(29), 1902953 (2019). https://doi.org/10.1002/adfm.201902953

86. H. Shao, K. Xu, Y.C. Wu, A. Iadecola, L. Liu et al., Unraveling the charge storage mechanism of $Ti_3C_2T_x$ MXene electrode in acidic electrolyte. ACS Energy Lett. **5**(9), 2873–2880 (2020). https://doi.org/10.1021/acsenergylett.0c01290

87. X. Hu, W. Zhang, X. Liu, Y. Mei, Y. Huang, Nanostructured Mo-based electrode materials for electrochemical energy storage. Chem. Soc. Rev. **44**(8), 2376–2404 (2015). https://doi.org/10.1039/c4cs00350k

88. I.A. Castro, R.S. Datta, J.Z. Ou, A. Castellanos-Gomez, S. Sriram et al., Molybdenum oxides–from fundamentals to functionality. Adv. Mater. **29**(40), 1701619 (2017). https://doi.org/10.1002/adma.201701619

89. Z. Su, W. Ren, H. Guo, X. Peng, X. Chen et al., Ultrahigh areal capacity hydrogen-ion batteries with MoO_3 loading over 90 mg cm^{-2}. Adv. Funct. Mater. **30**(46), 2005477 (2020). https://doi.org/10.1002/adfm.202005477

90. W. Zheng, J. Halim, A.E. Ghazaly, A.S. Etman, E.N. Tseng et al., Flexible free-standing $MoO_3/Ti_3C_2T_z$ MXene composite films with high gravimetric and volumetric capacities. Adv. Sci. **8**(3), 2003656 (2021). https://doi.org/10.1002/advs.202003656

91. H. Guo, D. Goonetilleke, N. Sharma, W. Ren, Z. Su et al., Two-phase electrochemical proton transport and storage in α-MoO_3 for proton batteries. Cell Rep. Phys. Sci. **1**(10), 100225 (2020). https://doi.org/10.1016/j.xcrp.2020.100225

92. Y. Shi, L. Peng, Y. Ding, Y. Zhao, G. Yu, Nanostructured conductive polymers for advanced energy storage. Chem. Soc. Rev. **44**(19), 6684–6696 (2015). https://doi.org/10.1039/c5cs00362h

93. S.K. Kim, J. Cho, J.S. Moore, H.S. Park, P.V. Braun, High-performance mesostructured organic hybrid pseudocapacitor electrodes. Adv. Funct. Mater. **26**(6), 903–910 (2016). https://doi.org/10.1002/adfm.201504307

94. A.M. Navarro-Suárez, J. Carretero-González, T. Rojo, M. Armand, Poly(quinone-amine)/nanocarbon composite electrodes with enhanced proton storage capacity. J. Mater. Chem. A **5**(44), 23292–23298 (2017). https://doi.org/10.1039/c7ta08489g

95. T. Sun, H. Du, S. Zheng, J. Shi, X. Yuan et al., Bipolar organic polymer for high performance symmetric aqueous proton battery. Small Methods **5**(8), 2100367 (2021). https://doi.org/10.1002/smtd.202100367

96. Z. Tie, S. Deng, H. Cao, M. Yao, Z. Niu et al., A symmetric all-organic proton battery in mild electrolyte. Angew. Chem. Int. Ed. **61**(8), 202115180 (2022). https://doi.org/10.1002/anie.202115180

97. A. Mukhopadhyay, Y. Jiao, R. Katahira, P.N. Ciesielski, M. Himmel et al., Heavy metal-free tannin from bark for sustainable energy storage. Nano Lett. **17**(12), 7897–7907 (2017). https://doi.org/10.1021/acs.nanolett.7b04242

98. H. Yao, F. Zhang, G. Zhang, H. Luo, L. Liu et al., A novel two-dimensional coordination polymer-polypyrrole hybrid material as a high-performance electrode for flexible supercapacitor. Chem. Eng. J. **334**, 2547–2557 (2018). https://doi.org/10.1016/j.cej.2017.12.013

99. M. Zhu, L. Zhao, Q. Ran, Y. Zhang, R. Peng et al., Bioinspired catechol-grafting pedot cathode for an all-polymer aqueous proton battery with high voltage and outstanding rate capacity. Adv. Sci. **9**(4), e2103896 (2021). https://doi.org/10.1002/advs.202103896

100. S. Kandambeth, J. Jia, H. Wu, V.S. Kale, P.T. Parvatkar et al., Covalent organic frameworks as negative electrodes for high-performance asymmetric supercapacitors. Adv. Energy Mater. **10**(38), 2001673 (2020). https://doi.org/10.1002/aenm.202001673

101. S. Haldar, R. Kushwaha, R. Maity, R. Vaidhyanathan, Pyridine-rich covalent organic frameworks as high-performance solid-state supercapacitors. ACS Mater. Lett. **1**(4), 490–497 (2019). https://doi.org/10.1021/acsmaterialslett.9b00222

102. K. Geng, T. He, R. Liu, S. Dalapati, K.T. Tan et al., Covalent organic frameworks: design, synthesis, and functions. Chem. Rev. **120**(16), 8814–8933 (2020). https://doi.org/10.1021/acs.chemrev.9b00550

103. Q. Jiang, N. Kurra, M. Alhabeb, Y. Gogotsi, H.N. Alshareef, All pseudocapacitive MXene-RuO_2 asymmetric supercapacitors. Adv. Energy Mater. **8**(13), 1703043 (2018). https://doi.org/10.1002/aenm.201703043

104. M. Boota, Y. Gogotsi, MXene-conducting polymer asymmetric pseudocapacitors. Adv. Energy Mater. **9**(7), 1802917 (2019). https://doi.org/10.1002/aenm.201802917

105. M. Boota, C. Chen, K.L.V. Aken, J. Jiang, Y. Gogotsi, Organic-inorganic all-pseudocapacitive asymmetric energy storage devices. Nano Energy **65**, 104022 (2019). https://doi.org/10.1016/j.nanoen.2019.104022

106. T. Xu, Z. Li, D. Wang, M. Zhang, L. Ai et al., A fast proton-induced pseudocapacitive supercapacitor with high energy and power density. Adv. Funct. Mater. **32**(5), 2107720 (2021). https://doi.org/10.1002/adfm.202107720

107. W. Sun, F. Wang, S. Hou, C. Yang, X. Fan et al., Zn/MnO_2 battery chemistry with H$^+$ and Zn^{2+} coinsertion. J. Am. Chem. Soc. **139**(29), 9775–9778 (2017). https://doi.org/10.1021/jacs.7b04471

108. Z. Tie, L. Liu, S. Deng, D. Zhao, Z. Niu, Proton insertion chemistry of a zinc-organic battery. Angew. Chem. Int. Ed. **59**(12), 4920–4924 (2020). https://doi.org/10.1002/anie.201916529

109. Z. Zhu, W. Wang, Y. Yin, Y. Meng, Z. Liu et al., An ultrafast and ultra-low-temperature hydrogen gas-proton battery. J. Am. Chem. Soc. **143**(48), 20302–20308 (2021). https://doi.org/10.1021/jacs.1c09529

110. F. Yue, Z. Tie, S. Deng, S. Wang, M. Yang et al., An ultralow temperature aqueous battery with proton chemistry. Angew. Chem. Int. Ed. **60**(25), 13882–13886 (2021). https://doi.org/10.1002/anie.202103722

111. T. Sun, H. Du, S. Zheng, J. Shi, Z. Tao, High power and energy density aqueous proton battery operated at –90 C. Adv. Funct. Mater. **31**(16), 2010127 (2021). https://doi.org/10.1002/adfm.202010127

112. Z. Liu, Y. Huang, Y. Huang, Q. Yang, X. Li et al., Voltage issue of aqueous rechargeable metal-ion batteries. Chem. Soc. Rev. **49**(1), 180–232 (2020). https://doi.org/10.1039/c9cs00131j

113. S. Wang, X. Zhao, X. Yan, Z. Xiao, C. Liu et al., Regulating fast anionic redox for high-voltage aqueous hydrogen-ion-based energy storage. Angew. Chem. Int. Ed. **58**(1), 205–210 (2019). https://doi.org/10.1002/anie.201811220

114. Y. Xu, X. Wu, H. Jiang, L. Tang, K.Y. Koga et al., A non-aqueous H_3PO_4 electrolyte enables stable cycling of proton electrodes. Angew. Chem. Int. Ed. **59**(49), 22007–22011 (2020). https://doi.org/10.1002/anie.202010554

115. K. Miyazaki, T. Shimada, S. Ito, Y. Yokoyama, T. Fukutsuka et al., Enhanced resistance to oxidative decomposition

of aqueous electrolytes for aqueous lithium-ion batteries. Chem. Commun. **52**(28), 4979–4982 (2016). https://doi.org/10.1039/c6cc00873a

116. Z. Hou, X. Zhang, X. Li, Y. Zhu, J. Liang et al., Surfactant widens the electrochemical window of an aqueous electrolyte for better rechargeable aqueous sodium/zinc battery. J. Mater. Chem. A **5**(2), 730–738 (2017). https://doi.org/10.1039/c6ta08736a

117. Y. Shao, M.F. El-Kady, J. Sun, Y. Li, Q. Zhang et al., Design and mechanisms of asymmetric supercapacitors. Chem. Rev. **118**(18), 9233–9280 (2018). https://doi.org/10.1021/acs.chemrev.8b00252

118. H. Wang, J. Li, X. Kuai, L. Bu, L. Gao et al., Enhanced rate capability of ion-accessible $Ti_3C_2T_x$-NbN hybrid electrodes. Adv. Energy Mater. **10**(35), 2001411 (2020). https://doi.org/10.1002/aenm.202001411

119. L.Y. Chen, Y. Hou, J.L. Kang, A. Hirata, T. Fujita et al., Toward the theoretical capacitance of RuO_2 reinforced by highly conductive nanoporous gold. Adv. Energy Mater. **3**(7), 851–856 (2013). https://doi.org/10.1002/aenm.201300024

120. H. Ma, D. Kong, Y. Xu, X. Xie, Y. Tao et al., Disassembly-reassembly approach to RuO_2/graphene composites for ultrahigh volumetric capacitance supercapacitor. Small **13**(30), 1701026 (2017). https://doi.org/10.1002/smll.201701026

121. R. Wang, Y. Sun, A. Brady, S. Fleischmann, T.B. Eldred et al., Fast proton insertion in layered $H_2W_2O_7$ via selective etching of an aurivillius phase. Adv. Energy Mater. **11**(1), 2003335 (2020). https://doi.org/10.1002/aenm.202003335

122. X. Chen, Y. Zhu, M. Zhang, J. Sui, W. Peng et al., N-butyl-lithium-treated $Ti_3C_2T_x$ MXene with excellent pseudocapacitor performance. ACS Nano **13**(8), 9449–9456 (2019). https://doi.org/10.1021/acsnano.9b04301

123. J. Tang, T. Mathis, X. Zhong, X. Xiao, H. Wang et al., Optimizing ion pathway in titanium carbide MXene for practical high-rate supercapacitor. Adv. Energy Mater. **11**(4), 2003025 (2020). https://doi.org/10.1002/aenm.202003025

124. Y. Yang, P. Zhang, L. Hao, P. Cheng, Y. Chen et al., Grotthuss proton-conductive covalent organic frameworks for efficient proton pseudocapacitors. Angew. Chem. Int. Ed. **60**(40), 21838–21845 (2021). https://doi.org/10.1002/anie.202105725

125. G. Wang, T. Chen, C.J. Gomez-Garcia, F. Zhang, M. Zhang et al., A high-capacity negative electrode for asymmetric supercapacitors based on a PMo_{12} coordination polymer with novel water-assisted proton channels. Small **16**(29), 2001626 (2020). https://doi.org/10.1002/smll.202001626